Nano Research

Open Access

Review Article

Cationic carbon dots: A novel class of mimetic enzymes

Xin Wu[1], Zhuang Tong[1], Yunliang Liu[1], Yi Yang[1], Yaxi Li[1], Yuanyuan Cheng[1], Jingwen Yu[1], Naiyun Liu[1] ✉, Chanyuan Jin[2] ✉, and Haitao Li[1] ✉

[1] *Institute for Energy Research, School of Chemistry and Chemical Engineering, Jiangsu University, Zhenjiang 212013, China*
[2] *Second Dental Center, Peking University School and Hospital of Stomatology, Beijing 100101, China*

Cite this article: *Nano Research*, **2025**, *18*, 94907333. https://doi.org/10.26599/NR.2025.94907333

ABSTRACT: Natural enzymes are highly efficient catalysts with strong substrate specificity, making them ideal for biomedical applications. However, they often face issues such as variability, high costs, challenging preparation processes, and difficulties in large-scale production. This has led to significant efforts in developing effective nanoenzymes and exploring their application potential. In recent years, carbon dots (CDs) have gained attention due to their strong fluorescence, excellent biocompatibility, and low cytotoxicity. Cationic CDs, which possess a positively charged surface, have shown the ability to mimic natural enzyme applications. The positive charge on the surfaces of these nanomaterials significantly influences their fluorescence, biological activity, and interactions with other biomolecules. Therefore, understanding how surface charge affects the performance of CDs is crucial for enhancing their usability. Considerable progress has been made in the design, synthesis, and mechanistic research of enzyme-like cationic CDs, as well as their advanced applications. This article reviews the latest research on the design structure, catalytic mechanisms, biosensing capabilities, and biomedical applications of enzyme-like cationic CDs. First, we review the synthesis strategies for cationic CDs and how surface charge influences their physical and chemical properties. Next, we highlight various applications of these cationic CDs, demonstrating their use in areas such as detection, biomedical applications (including antibacterial agents, gene carriers, and therapeutic agents), catalysis, and more. Finally, we discuss the challenges and obstacles faced in the development of cationic CDs and look forward to exploring new applications in the future.

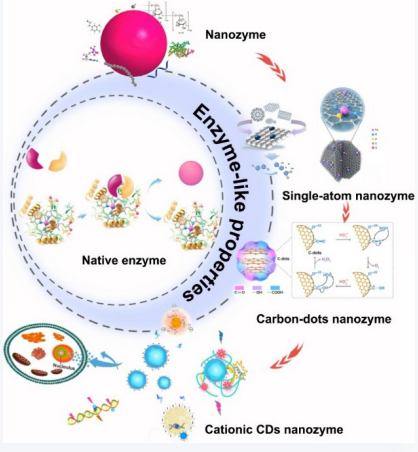

KEYWORDS: cationic carbon dots, enzyme-like, catalysis, applications, nanomaterials

1 Introduction

Natural enzymes are proteins or RNAs functioning as highly efficient biological catalysts in multiple physiological processes within living organisms. However, they possess certain drawbacks, including high costs associated with their isolation, purification and storage, lack of recyclability, and extreme susceptibility to environmental conditions, all of which impair their catalytic effectiveness and hinder their practical applications. Nanozymes, as emerging nanomaterials with enzyme-like activities, have overcome some of the shortcomings of natural enzymes and are favored with easy preparation, high catalytic efficiency, low cost, and high stability. However, the catalytic efficiency of nanozymes can't match that of natural enzymes. Besides, comprehension of the precise catalytic mechanisms underlying nanozymes is still in the initial stages, limiting the precision in designing targeted therapies and anticipating prolonged biological consequences [1–3]. Single atom nanozymes are a novel type of nanozyme with active sites composed of individual metal atoms, similar to the active sites of natural metalloenzymes. They can catalyze the reaction of enzyme substrates under physiological conditions and possess catalytic efficiency and enzyme-promoted reaction kinetic properties similar to natural enzymes. However, both nanozymes and single-atom nanozymes face challenges in balancing good physicochemical properties and enzymatic activity [4–7].

Carbon dots (CDs), a well-known luminescent carbon-based nanomaterial, have received growing attention from the time of their discovery. They are usually sphere-shaped nano-crystals smaller than 10 nm [8]. In contrast to conventional semi-conducting quantum dots (QDs), the CDs have a number of oxy-functional groups, like carboxyl, hydroxyl, or epoxy functional

Received: December 4, 2024; **Revised:** February 23, 2025
Accepted: February 25, 2025

✉Address correspondence to Naiyun Liu, liuny@ujs.edu.cn; Chanyuan Jin, jinchanyuanjcy@163.com; Haitao Li, liht@ujs.edu.cn

groups, which offer a high degree of selectivity and the ability to chemically interact with additional chemical as well as biological entities [9–12], and also have many extraordinary properties, including abundant photoluminescence properties [13, 14], easy surface functionalization, chemical stability [15], photostability, excellent biocompatibility [16], low cytotoxicity [17], and excellent water solubility [18]. These special properties have been widely used in biomedical and chemical applications [19, 20].

Owing to the presence of some oxygen functional groups on the surface, normal CDs show a negative surface potential. While doped and surface-modified CDs usually exhibit positive surface potentials from nitrogen-containing organic precursors [21, 22]. These CDs with a large number of positively charged surface functional groups are called cationic CDs. Cationic CDs, due to their unique physicochemical properties and surface functional groups, can exhibit enzyme-like catalytic activity. Therefore, they can be regarded as a special kind of nanoenzymes. Furthermore, cationic CDs with surface defects and unpaired electrons have more active sites, which can provide rapid electron transport effects. This leads to improved catalytic performance, allowing them to mimic the catalytic action of natural enzymes. As a result, these modified CDs show promise as substitutes for natural enzymes in biomedical applications.

The surface positive charge of nanomaterials significantly affects fluorescence, bioreactivity, and interaction with biomolecules. For instance, in the application of CDs as an antibacterial agent, cationic CDs are more easily attracted to bacterial cell membranes, which typically carry a net negative charge, through electrostatic interactions [22]. This attraction enhances their antibacterial activity, making cationic CDs suitable for use as biomedical materials. Additionally, these cationic CDs exhibit enzyme-like activities, such as catalase-like activity, which enables their use in biosensors, including those for glucose monitoring. Although various review articles summarize the preparation and applications of CDs [23, 24], only one review is focused on cationic CDs. Mohammadinejad et al. described the precursors, structures, and properties of cationic CDs in detail, demonstrated various applications of these materials in gene delivery, and also discussed the potential of CDs as traceable gene delivery systems [25]. However, recent researches on cationic CDs have reported numerous different synthesis methods and applications. Hence, some organization and in-depth analysis thereof are necessary.

In this review, we present a summary of the synthesis methods for cationic CDs, the influence of surface charge on CDs performances, as well as the applications for cationic CDs in recent years. The influence of surface charge on the performances of CDs, which include optical, chemical, biological, and physical characteristics, is comprehensively described. Applications of cationic CDs are categorized and summarized thoroughly, covering fluorescent sensors, biomedicine (imaging, antibiosis, therapy, non-viral gene vectors), catalysis (including photocatalysis and electrocatalysis), physical adsorption and separation (Fig. 1). We also conclude with a comprehensive summary of some of challenges and barriers faced during the development of cationic CDs, as well as an outlook regarding further exploration for new applications.

2 Synthetic methods and the properties of cationic CDs

Cationic CDs have garnered significant attention due to their adjustable enzyme activity, microbial adhesion, and excellent biocompatibility across a broad spectral range [26]. In particular, CDs with an sp^2 hybrid structure have demonstrated a strong ability to generate reactive oxygen species. Nitrogen doping in these CDs enhances their peroxidase activity, making them more effective as nanomaterials. Furthermore, the intrinsic activity of carbon nanomaterials can be further improved by using thiourea as a source of sulfur.

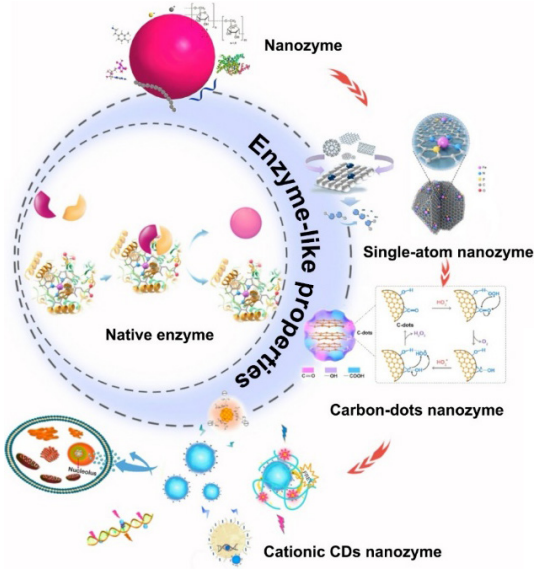

Figure 1 Development of nanomaterials with enzyme-like properties.

The synthesis methods for cationic CDs are similar to those used for traditional CDs and are typically categorized into two approaches: top-down and bottom-up methods. For the synthesis and surface passivation of cationic CDs, positively charged compounds or polycations are commonly employed. There has been significant focus on synthetic polymers that contain amines, such as polyethylene imine (PEI), chitosan, poly-L-lysine (PLL), and poly(amidoamine) (PAMAM). The top-down methods include techniques such as laser ablation, ultrasonication, electrochemical oxidation, and chemical oxidation. On the other hand, bottom-up methods consist of microwave-assisted pyrolysis, solvothermal methods, and hydrothermal carbonization. The size of cationic CDs synthesized by microwave is easily controllable, with a relatively uniform size distribution and short reaction time. Although the size distribution of CDs obtained through thermolysis is wide, the preparation is low in cost and easy to operate. The synthesis of CDs using solvothermal method is cost-effective and has high quantum efficiency. Therefore, these three methods are mostly used methods for preparing cationic CDs [25]. Here, we discuss in detail the characteristics of different CDs obtained by these three methods and the impact of surface charge on the characteristics of different CDs obtained by different preparation methods.

2.1 Microwave synthesis

Microwave technology has emerged as a process of great importance in synthetic chemistry. Cationic CDs prepared by microwave heating is to rely on microwave to make polar molecules vibrate rapidly to generate heat, so that the reaction system heating, accelerate the shrinkage of the carbon source, carbonisation and surface modification to form CDs, the cationic CDs prepared in this way are small and homogeneous in size, with a lot of oxygen-containing functional groups on the surface, and

have a good fluorescence performance. Ma et al. proposed a simple method of microwave heating for the synthesis of peptide dendritic CD-based ternary nanoparticles (pCBMA (CD-D/DOX)) [27]. In the synthesis process, glucose and varying amounts polyethylene glycol 200 (PEG200) were dissolved into distilled water forming a clear solution. Then the beaker was heated in an 800 W microwave oven for 3 min. As reaction time increased, solution changed color from colorless into deep brown, implying CDs formed.

Chowdhury et al. reported for the first time that CDs were obtained from chitosan gels by microwave heating, and the gels were stable and non-degradable, so that the raw material for the preparation of CDs had a longer shelf life [28]. The CD Zeta potential is +27 mV and has good photoluminescence (PL) properties. Its particle size ranges from 0.6 to 8.7 nm. Sahiner et al. synthesized nitrogen-doped (N-) and sulfur-doped (S-)CDs using arginine (A), lysine (L), histidine (H), cysteine (C) and methionine (M) as source materials by simple 1–4 min micro-wave procedure (Fig. 2), all four amino acid carbon dots showed positive charges, except for cysteine-derived CD (C-CD) which exhibited negative surface charges [29]. They have higher quantum yield (QY) values compared to undoped materials. These amino acid-based CDs are non-toxic and biocompatible due to their –COOH, –NH, and –SH groups.

2.2 Thermolysis

Pyrolysis is widely used as a method of cationic CDs synthesis because of the lower cost and simplicity of operation. Guo et al. used citric acid along with l-glutathione (GSH) as a source of carbon and dopant elements and added polyene-polyamines (PEPA) [30]. The p-CD with positively charged amine-rich surface was prepared by simple pyrolysis (Fig. 3(a)), and the resulting cationic CDs retained their intrinsic luminescent properties while exhibiting strong quenching ability against fluorophore-modified DNA. The most prevalent and possessing important physiological functions polyamine include putrescine, cadaverine, spermidine, and spermine, which consist of small aliphatic hydrocarbon molecules bearing primary and secondary amines with a net positive charge at physiological pH. Jian et al. synthesized polyamine-modified carbon quantum dots (CQD_{Spds}) by pyrolysis of solid spermidine (Spd), which exhibited higher solubility and yield than other biopolyamines [31]. However, Chen et al. recently showed that CQD_{Spds} causes histopathological damage, including hepatic steatosis and mild mixed inflammatory cell infiltration; it showed significant cytotoxicity in human embryonic kidney (HEK293) cells, inducing oxidative stress but not activating NOD-like receptor family pyrin domain containing 3 (NLRP3) inflammasome; reduced liver function was observed in CQD_{Spds}

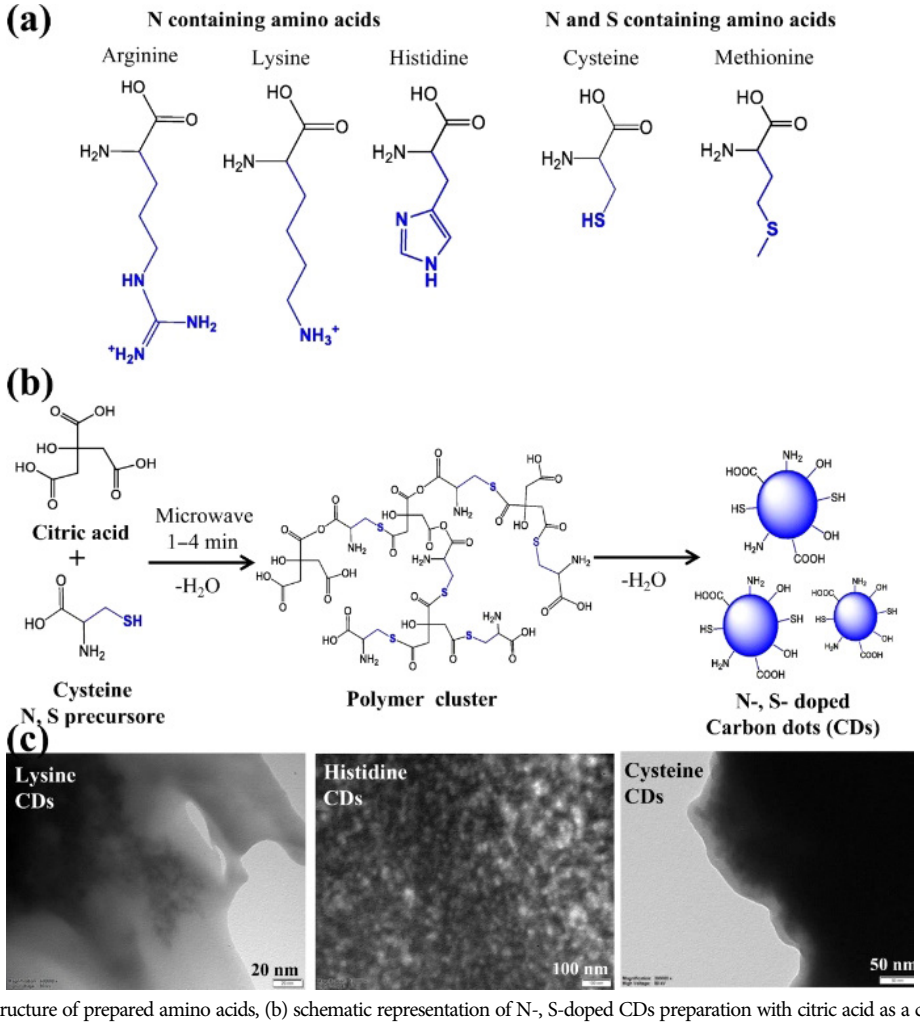

Figure 2 (a) Molecular structure of prepared amino acids, (b) schematic representation of N-, S-doped CDs preparation with citric acid as a carbon source and cysteine as an S and N doping source, (c) TEM images of amino acid derived CDs. Reproduced with permission from Ref. [29], © Springer Science Business Media, LLC, part of Springer Nature 2019.

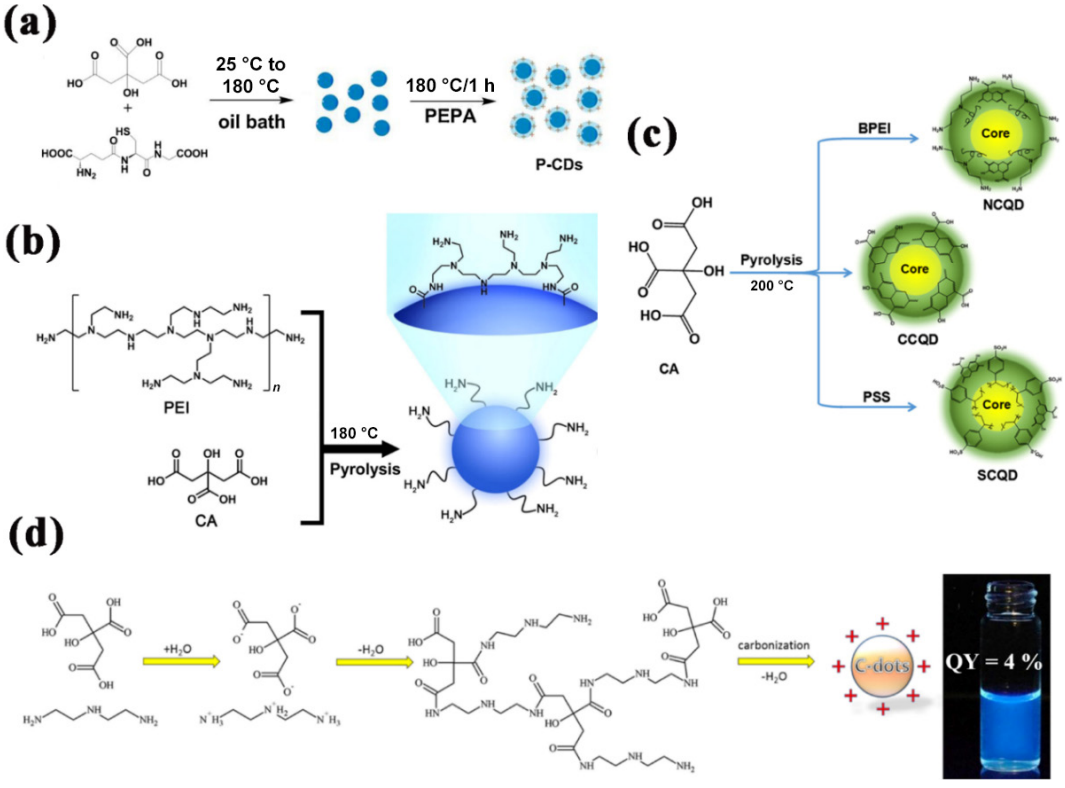

Figure 3 Schematic synthesis of (a) P-CDs [30]. Reproduced with permission from Ref. [30], © Elsevier B.V. All rights reserved 2018. (b) CQDs modified by PEI [36]. Reproduced with permission from Ref. [36], © Elsevier Ltd. All rights reserved 2015. (c) Carboxy CQD (CCQD), amino CQD (NCQD) and sulfonated CQD (SCQD) [37]. Reproduced with permission from Ref. [37], © Elsevier B.V. All rights reserved 2018. (d) Amine-modified CDs [40]. Reproduced with permission from Ref. [40], © Elsevier B.V. All rights reserved 2017.

treated mice. Therefore, it is important to consider the risk of toxicity in the subsequent preparation and application of this type of cationic CQDs [32, 33].

Compared to other methods, the pyrolysis method for the formulation of cationic CDs is somewhat demanding in terms of carbon source, requiring organic molecules with a low melting temperature as the carbon source. Moreover, it is typically carried out at elevated temperatures [34, 35]. However, Shi et al. prepared CQDs by low-temperature pyrolysis using CA and polyethyleneimine (PEI) as carbon sources and co-reactants, where citric acid (CA) was often used as a carbon source due to the ability of carboxyl groups to promote dehydration and carbonization (Fig. 3(b)) [36]. Sun et al. prepared three CQDs with different functional groups by pyrolysis, namely carboxy CQD (CCQD), amino CQD (NCQD) and sulfonated CQD (SCQD) [37], CCQD was prepared by direct pyrolysis of CA, SCQD was prepared by using CA and poly(sodium 4-styrenesulfonate) (PSS) as precursors via a one-step pyrolysis method, while NCQD was synthesized in the existence of branched polyethyleneimine (BPEI) through low-temperature thermolysis of CA (Fig. 3(c)). The addition of BPEI gives NCQD an $-NH_2$ group, making the CDs positively charged, while CCQD with the presence of abundant –COOH groups and SCQD with the introduction of multivalent $-SO_3^{2-}$ had more negative Zeta potential values.

The size distribution of CQDs prepared by conventional pyrolysis is wide, while the PL properties of quantum dots depend on the size of QDs [38], so the microwave-assisted pyrolysis method is becoming more and more popular. This preparation method has short reaction time and makes the size of CQDs easily controllable and uniform in size distribution. In addition, microwave-assisted pyrolysis of cationic CDs were prepared in the general anoxic or oxygen-free environment, using of microwave heating to cause the decomposition of the carbon source, which will make its structure more graphitised, with high surface charge density and better stability. Zhang et al. synthesized amine-terminated CDs ($CDs\text{-}NH_2$) from l-asparagine and ethylenediamine (EDA) by microwave-assisted pyrolysis [39]. EDA makes most of the carboxyl amidation of l-asparagine, and the final CDs are wrapped by amino group to be positively charged, and this method had enough time for thorough pyrolysis so that no further purification was required, and the fluorescence QY at 360 nm was 11.4%. Jiri et al. chose diethylenetriamine (DETA) as the surface passivation agent, and synthesized amine-modified CDs by one-step microwave pyrolysis using CA as the carbon source [40]. The stable mediation by amine groups on the CDs surface at neutral pH allowed the CDs to have a positive surface charge, and they exhibited good water solubility. The aqueous solution of the CDs showed blue fluorescence with a QY value of 4% (Fig. 3(d)). Rohan et al. also used CA as a carbon precursor, but synthesized N-doped cationic CDs using PEI as a capping agent and fluorescence enhancer, whose aqueous solution showed a higher QY of 46% [41].

Usually the use of N-doping or N-containing passivators increases the QY of the CDs, but the reason for why CDs prepared by CA and specific amines has such a high QY is not yet clarified. Since CD formation, passivation of the surface as well as the development of nanoparticles occur at the same time without clear boundaries, the pyrolysis time is also considered to be an important

factor affecting the QY of CDs [42, 43]. The CDs with a relatively low QY may be the result of frequent dialysis time extension of water changes leading to smaller CDs and loss of fluorescent molecules [44].

2.3 Solvothermal method

The solvothermal method is another common method for the synthesis of cationic CDs. The QY of the prepared N-CQDs tends to be relatively low due to the small proportion of nitrogen in common biomass materials. In contrast, N-CQDs prepared by the bottom-up solvothermal method have higher yields due to the high nitrogen content from the use of a molecular nitrogen source. Qian et al. synthesized N-CQDs by solvothermal using different diamine carbon chains as nitrogen precursors and adding carbon tetrachloride, while comparing the effects of nitrogen percentage and nitrogen type on the fluorescence of N-CQDs [45]. The doping of nitrogen atoms as active sites significantly improved the fluorescence of N-CQDs. They also optimized the solvothermal conditions and reaction time in order to obtain the best quantum yield and good monochromatic dispersion.

Lin et al. used a solvent thermal method to synthesize CDs using anhydrous citric acid and PEG 1500 as the carbon source and passivation agent, and the quantum yield of CDs obtained by this method (21%) was higher than that of quantum nanodots synthesized by the reflux route (17%) [46]. Wu et al. synthesized CDs of ultra-small dimensions (ca. 3.3 ± 0.4 nm) with long alkyne-linked quaternary ammonium groups on their surfaces and strong positive charges (Zeta potential: ca. +33.1 ± 2.5 mV) by solvothermal using a 1:2 volume ratio of dimethyloctadecyl (trimethoxysilyl) propylammonium chloride (Si-QAC) and glycerol [47].

Nevertheless, the majority of organic solvents are both toxic and costly, as well as potentially causing serious harm to the health of the human body. Compared to that, the use of water is a kind of green and inexpensive solution, therefore the water-thermal methods are more used in the preparation of cationic CDs. In 2016, Zhou et al. synthesized multifunctional CDs using hydrothermal carbonization of alginate, in which alginate acts as both a carbon source and a cationic agent, and the prepared CDs are positively charged, have aqueous dispersion, and exhibit a strong and stable fluorescence [48]. Yang et al. synthesized cationic CDs using folic acid (FA) and PEI by simple, low-cost hydrothermal carbonization (Fig. 4(a)). The CDs exhibit stable and strong PL properties and relatively high QY (42%). The presence of CDs reduced the toxicity of PEI and allowed its direct use for cell imaging [49].

In general, heteroatom doping can improve and modify the

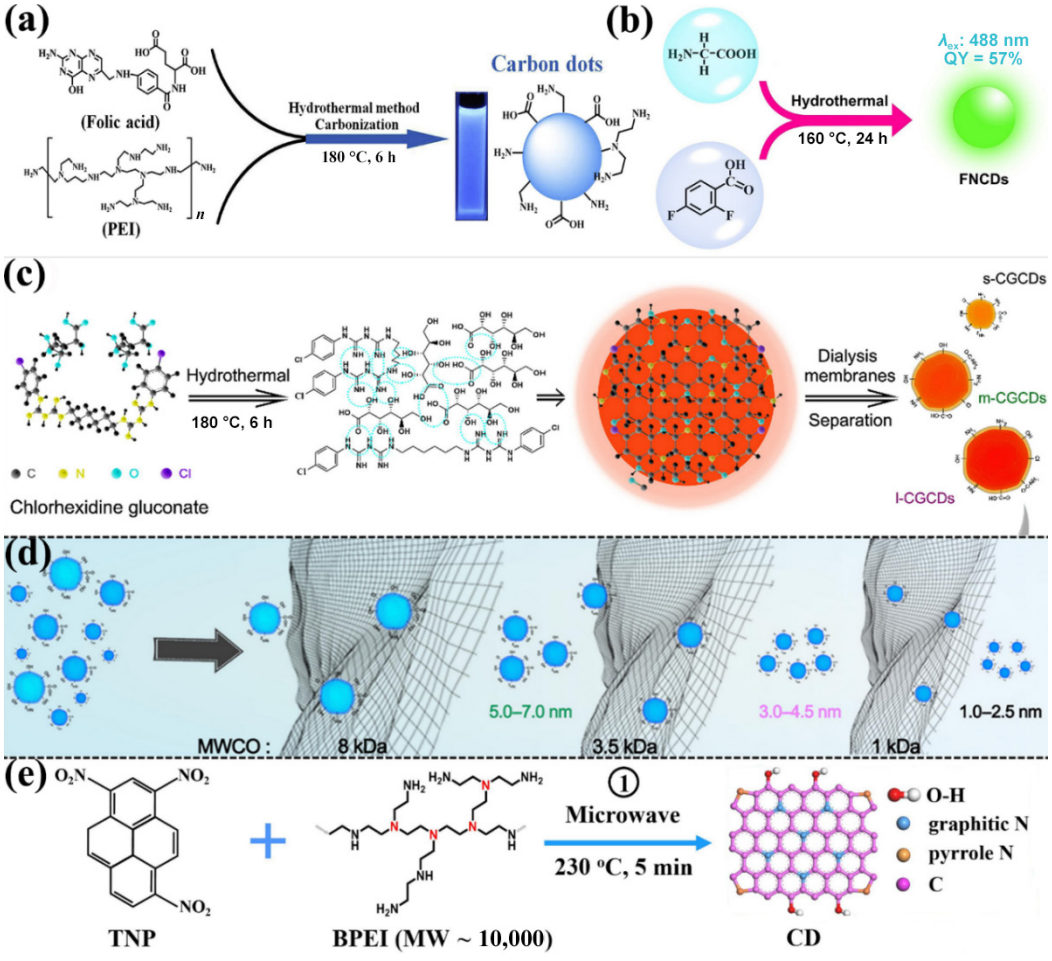

Figure 4 The synthesis process of (a) CDs with FA and PEI [49]. Reproduced with permission from Ref. [49], © Elsevier Inc. All rights reserved 2016. (b) Construction of FNCDs [56]. Reproduced with permission from Ref. [56], © Elsevier B.V. All rights reserved 2020. (c) Schematic representation of the strategy employed for the preparation of s-CGCDs, m-CGCDs, and l-CGCDs [57]. (d) Schematic diagram of separating different particle sizes through dialysis membranes with different cut-off molecular weights [57]. Reproduced with permission from Ref. [57], © Elsevier Inc. All rights reserved 2020. (e) The microwave-assisted synthesis of NIR-II responsive CDs [58]. Reproduced with permission from Ref. [58], © Elsevier B.V. All rights reserved 2019.

performance of CDs. Doping with N can create defective sites that eventually enhance the fluorescence performance on CDs [50–52]. Elemental fluorine (F) exhibits the greatest electrical negativity among any element and is prone to hydrogen bond formation, which improves luminescence stability [53–55], preparation of N and F co-doped CDs can further improve its emission wavelength, surface charge and yield. Li et al. prepared such F and N co-doped CDs (FNCDs) using hydrothermal method (Fig. 4(b)). FNCD has a maximum photoluminescence emitting wavelength at 502 nm and an optimal excitation wavelength at 466 nm, respectively. Especially, their quantum yields in aqueous solutions are as high as 57%. They exhibit good fluorescence stability under different pH, temperature, ionic strength and guest molecule conditions [56].

Sun et al. used hydrothermal synthesis of chlorhexidine gluconate CDs using carbonated chlorhexidine gluconate (CG), CG provided the carbon and nitrogen source [57], they also used a separation membrane method to separate the CDs into different particle sizes, including ~ 2.0 nm small particle size CGCDs (s-CGCDs), ~ 3.9 nm intermediate particle size CGCDs (m-CGCDs) and ~ 5.3 nm large particle size CGCDs (l-CGCDs) (Figs. 4(c) and 4(d)). Due to the similarity of the precursors, these three types of CGCDs have similar characteristics, however, there are variations in PL properties and bacteriostatic effects.

In addition, microwave-assisted hydrothermal approaches use high temperatures generated rapidly by microwave radiation, enabling dehydration and carbonization of the carbon source within a few minutes. Geng et al. synthesized CDs with good photothermal effects using ultrafast microwave-assisted hydrothermal methods within the second near-infrared window (Fig. 4(e)). Its surface is positively charged, which allows it to be electrostatically assembled on each side of the negativity charged WS_2 nanosheets [58].

Different synthesis methods lead to variations in the carbon core and functional group structures of CDs. High crystallinity CDs are primarily derived from larger carbon structures such as graphite rods, graphene, and carbon nanotubes through processes like acid oxidation, electrochemical stripping, laser ablation, and microwave stripping. The diverse surface functional groups (mainly nitrogen-containing functional groups found in cationic CDs), and the presence of heteroatom doping sites in CDs are largely attributed to the variety of precursor elements used. By optimizing factors such as the reaction precursor, duration, solvent, and temperature, it is possible to control the chemical structure, composition, and size of cationic CDs.

3 Applications of cationic carbon dots

The positive surface charge of nanomaterials greatly influences fluorescence, bioreactivity, and interactions with biomolecules [59–66]. These characteristics enable cationic CDs to be utilized in sensors, biomedicine, and catalysis [67, 68].

3.1 Sensor

Cationic CDs have received extensive attention for their excellent optical properties and enzyme-like activity, especially catalase-like activity, in the sensing field [69–75]. Based on the high affinity of Co-CDs to H_2O_2, Lu et al. constructed a colorimetric sensor for detecting glucose by combining Co-CDs with glucose oxidase. Due to the high catalytic activity and the cascade strategy, it has a good linear relationship in the range of 0.500–200 μM, and the detection limit is 0.145 μM. The biosensor achieves accurate detection of glucose in human serum samples [76].

Yang et al. reported that cationic CDs and neutral red (NR) aggregated with negatively charged hyaluronic acid (HA) along linear chains by electrostatic adsorption, establishing an electrostatically controlled ratiometric fluorescence analysis method for hyaluronidase (HAase) detection (Fig. 5(a)). The shortening of the distance separating the cationic CDs from the NR results in a significant fluorescence resonance energy transfer (FRET) between the cationic CDs and the NR. Under this condition, there will be a red fluorescence which is considered to detect the initial state of HAase. Linear HA is degraded by HAase into low molecular weight fragments, and insufficient inhibition of small HA fragments to counteract hydrostatic repulsion forces between cationic CDs and NR, and absorption of fluorescent components progressively segregates from nanoclusters. Therefore, between cationic CDs and NR, FRET becomes weaker, with an increase in fluorescence emission around 525 nm and a decrease towards 630 nm, and a change in fluorescence color is observed from red to yellowish-green, with the naked eye, even in the presence of UV irradiation, which facilitates semi-quantitative measurements with limited instrumentation [77]. Pushap et al. developed a simpler, more sensitive ratiometric fluorescent sensor to detect the HAase, and established a FRET mechanism by adsorbing cationic CDs and naphthalimides onto negatively charged HA (Fig. 5(b)). It has a detectable limit of 0.09 U/mL, below the level of HAase in normal human body fluids and can be used to diagnose HAase-related diseases [78].

In addition, cationic CDs have been used to detect copper ions. The presence of excess copper ions in blood often harms our DNA which may even contribute to a variety of diseases including Alzheimer's disease [79, 80], amyotrophic lateral sclerosis [81] and Parkinson's disease [82–84]. Therefore, the adoption of effective ways to monitor copper ion levels is very important to keep our bodies safe. A simple and green approach to synthesize N-doped cationic CDs was used by Feng et al [85]. The CDs have biocompatible and pH-sensitive luminescence properties. Cu^{2+} will coordinate to functional groups on the surface of P-CDs, and their combining interactions lead to a constant shape as well as a statically quenched behavior of the cationic CDs (Fig. 5(c)). The linear range of the response of cationic CDs to Cu^{2+} selectivity and sensitivity is 0.05–8 μM, and the detection limit is 0.035 μM. At the same time, assay results showed that Cu^{2+} was well detected in complex matrices from serum samples. In addition to monitoring Cu^{2+} in living organisms, N-doped cationic CDs have also been applied to the detection and extraction of Cu^{2+} in industrial mineral processing. Thomas et al. prepared positively charged N-CQDs adsorbed onto graphene oxide (GO) via charge interactions to form surface-active complexes (GO/CQDs), with the surface charge of GO was shielded by the N-CQDs, thereby enhancing their group affinity to the toluene-water interface [86]. As soon as the sample is attached to the oil-water interface, the N-CQDs are able to measure the copper ion concentration in the aqueous subphase by quantifying the extent of their fluorescence quench. And the validity of the copper ion concentration is not affected by the presence of stable GO.

Wang et al. fabricated a new type of FRET-ratio fluorescent probe via electrostatic attraction from positively charged amino CDs to negatively charged Au nanoclusters (Au NCs) for the detection of Cu^{2+} and Pb^{2+} (Fig. 5(d)) [87]. The fabricated probe

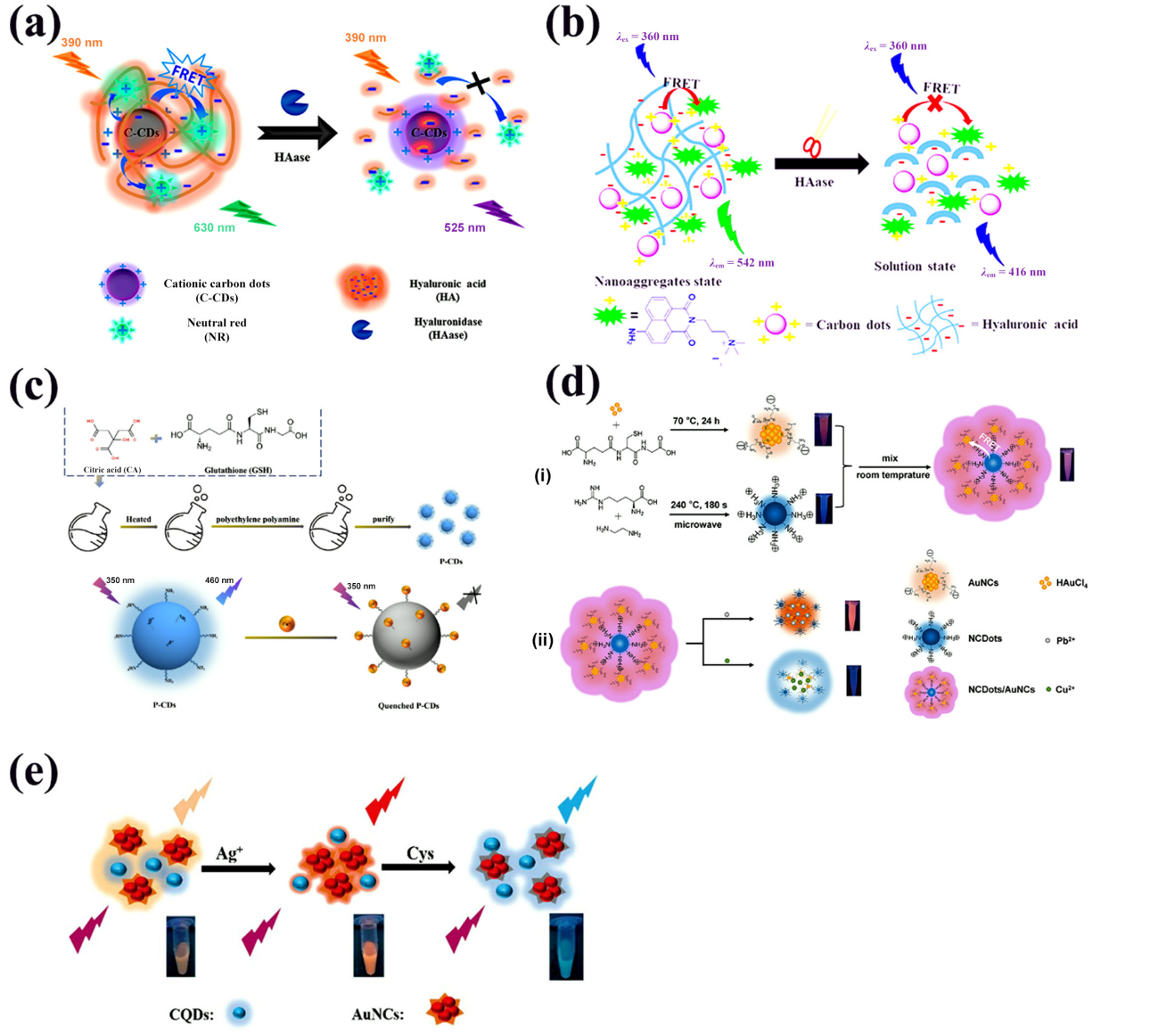

Figure 5 (a) Schematic illustration for the electrostatic-controlled ratiometric fluorescence assay in response to HAase [77]. Reproduced with permission from Ref. [77], © American Chemical Society 2017. (b) Graphical representation of the FRET mechanism for the sensing of hyaluronidase [78]. Reproduced with permission from Ref. [78], © Raj, P. et al. Licensee MDPI, Basel, Switzerland 2021. (c) The detection of Cu^{2+} based on the prepared P-CDs using one-pot melting step [85]. Reproduced with permission from Ref. [85], © Korean Chemical Society, Seoul & Wiley-VCH GmbH 2020. (d) Schematic diagrams showing the preparation of N-CDots/AuNCs probe and ratiometric fluorescent detection of Pb^{2+} and Cu^{2+} by the prepared probe [87]. Reproduced with permission from Ref. [87], © Elsevier B.V. All rights reserved 2018. (e) Schematic illustration of the detection of Ag^+ and L-cysteine with a dual-emissive nanosystem of CQDs and Au NCs [88]. Reproduced with permission from Ref. [88], © The Royal Society of Chemistry 2018.

showed double-emission peaks observed at 440 and 565 nm, and effective FRET could be produced at a single 380 nm excitation wavelength (Fig. 5(e)). For CDs, the blue fluorescence remains stable, while for the Au nanoclusters, the red fluorescence is enhanced with Pb^{2+} and extinguished by Cu^{2+}, resulting in a change in the fluorescence ratio that can be used to detect copper and lead ions in real water samples. This same FRET fluorescent probe designed by compounding cationic CDs with Au NCs was also used for the visual detection of Ag^+ and cysteine (Cys) in paper by Han et al. Ag^+ enhances the orange emission of Au NCs, which is gradually quenched in the presence of Cys (Fig. 5(f)). In addition, some research groups have synthesized composites of CQDs/Au nanoparticles (AuNPs), which are also compounded by electrostatic forces [88].

Wu et al. developed a simple, convenient and sensitive sensor platform to detect organophosphorus pesticides (OPs) on the basis of FRET analysis between CQDs and AuNPs [89]. The principle of FRET-based sensing platform for OPs determination, as shown in Fig. 6(a). Using n-acetyl l-cysteine-cap AuNPs (NAC-AuNPs) and highly fluorescent cationic CDs, Dong et al. proposed a new far-red for l-cysteine (L-Cys) ratio FRET fluorescent probe (Fig. 6(b)). The emission intensity exhibited well linear correlation with L-Cys concentration at 539 and 630 nm over the range from 1.0 to 110 μM, and the limitation of detection was 0.16 μM [90]. Li et al. modified AuNPs (*β*-CD@AuNPs) with *β*-cyclodextrin to be negatively charged and then complexed with positively charged CQDs by electrostatic interaction, and the prepared CQDs/*β*-CD@AuNPs nanosensor can be used to detect cholesterol in pig

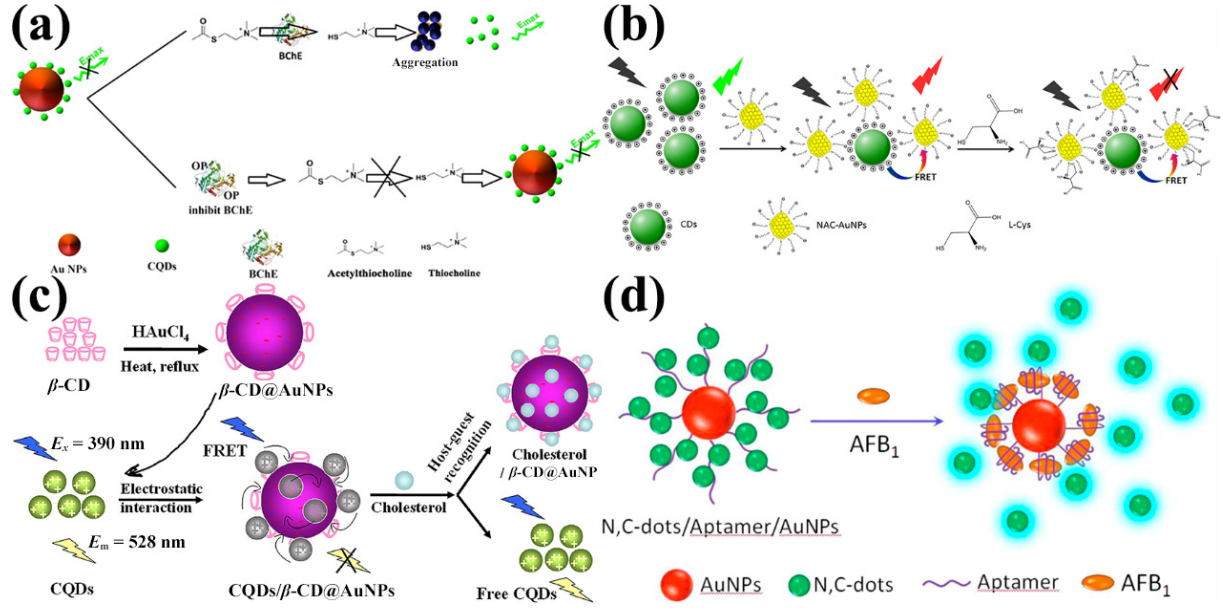

Figure 6 (a) The principle of FRET-based sensing platform for OPs determination [89]. Reproduced with permission from Ref. [89], © Published by Elsevier B.V 2017. (b) Schematic illustration of the far-red fluorescent sensing for ratiometric detection of L-cysteine based on FRET system of CDs and NAC-AuNPs [90]. Reproduced with permission from Ref. [90], © Published by Elsevier B.V. 2019. (c) The FRET occurred between CQDs and β-CD@AuNPs under the role of static electricity. And CQDs was replaced by cholesterol, based on the specific host-guest recognition between the inner cavity of β-CD and cholesterol, the FRET could be interrupted, and then the fluorescence of CQDs was turned on [91]. Reproduced with permission from Ref. [91], © Published by Elsevier B.V. 2019. (d) AFB1 assay strategy [92]. Reproduced with permission from Ref. [92], © Elsevier B.V. All rights reserved 2015.

serum (Fig. 6(c)) [91]. In the field of food safety control, an ultrasensitive biosensor with aptamers for detecting aflatoxin B1 was successfully carried out by Wang et al [92]. Positively charged N-doped CDs are mounted on aptamer-modified Au nanoparticles (aptamer/AuNPs). The specific interaction between AFB1 and aptamer leads to the release and fluorescence recovery of N-doped CDs, with recovered fluorescence intensity directly proportional to added aflatoxin B1 (AFB1) concentration (Fig. 6(d)), which allows the sensor to be highly sensitive and selective for the detection in true samples of AFB1. A summary of recently reported cationic CDs based sensors is given in Table 1.

In sensing applications, the positively charged surface of cationic CDs can specifically bind to negatively charged substances through electrostatic interaction, resulting in high selectivity for specific analytes [93]. In addition, they have fluorescent properties, and the fluorescence intensity and wavelength change when affected by the environment, and the signal is easy to detect, making them valuable biosensing materials. The sensing principle is usually based on specific interactions between the surface functional group or targeting moiety and the analyte, which leads to a change in the photoemission properties of the cationic CDs, thus achieving high sensitivity and selectivity for the detection of specific molecules. Cationic CDs can be used for the detection of metal ions, such as mercury ions, which bind to cationic carbon dots and cause fluorescence bursts, enabling highly sensitive detection of mercury ions; and for the detection of biomolecules, such as adenosine triphosphate (ATP), which is negatively charged and binds to cationic CDs to change fluorescence, enabling the determination of ATP concentration. This is of great importance in biological analysis and clinical diagnosis.

3.2 Biomedicine

Most natural enzymes are proteins, which can lead to certain inherent drawbacks, such as variability, susceptibility to loss of activity, cumbersome purification processes, and challenges in storage and recycling [94–99]. In contrast, cation CDs enzyme-like materials offer enhanced physical and chemical stability, versatility, and recyclability [100, 101]. Researchers have discovered that CDs possess good enzyme activity, effective hydroxyl radical scavenging capabilities, and superior fluorescence properties, making them suitable for biomedicine applications. This section explores the use of CDs in biomedicine across four key areas: imaging, antibiosis, therapy, and non-viral gene carrier.

3.2.1 *Imaging*

Imaging nanoenzyme refers to nanoenzyme applied in the field of imaging, which has both the nanoenzyme activity and imaging function. It not only catalyzes specific biochemical reactions, but also enables real-time monitoring and localization through imaging technologie. CDs have received lots of attention in building imaging probe frameworks due to their high biocompatibility, green synthesis, low toxicity, luminescence properties, and easy surface functionalization [102–105]. Through specific excitation light irradiation, the CDs nanoenzyme can emit fluorescence to realize the imaging of biomolecules, cells or tissues, and provide visualization means for disease diagnosis, biological process monitoring and so on [56]. We describe here in three parts: enhancement of imaging signals, targeted imaging, and imaging-guided therapy monitoring.

(1) Enhanced imaging signal: In general, variations in the morphology of chromosomes may indicate the cell division process. To understand every phase of that cell cycle is crucial to determine the mechanisms that regulate the process, whereby unusually divided cells are often a sign of many diseases (e.g., cancer) [106]. Therefore, using probes for live cell imaging can help us visualize the process of cell division more intuitively. Cell cycle assays are based on positively charged fluorescent dyes which are

Table 1 The application of cationic CDs in sensing

Cationic CDs	Synthesis approach	Precursors	Zeta potential (mV)	FLQY (%)	Ex/Em (nm)	Analytes	Sensing mode	LOD (nM)	Ref.
N, C-dots	Hydrothermal	Pancreatin	/	/	370/445	Aflatoxin B1	Fluorescence	0.016	[52]
CDs	Hydrothermal	4-Aminobenzoic acid, m-phenylenediamine	+15.4	59.6%	414/539 630	L-Cysteine	Ratio	160	[50]
CQDs	Sonication	Cetylpyridinium chloride	/	/	390/528	Cholesterol	Fluorescence	343.48	[51]
N, S co-doped carbon nanodots	Hydrothermal	Citric acid, thiourea	+18.8	/	400/420–610	Living cancer cells	Fluorescence	5 cells/mL	[46]
N-CDots	Microwave	Arg, ethylenediamine	+17.7 ± 1.03	/	380/440 565	Pb^{2+}/Cu^{2+}	Ratio	20,000	[47]
C-CDs	Sonication	Cetylpyridinium chloride	+39.2	/	390/525	HAase	Ratio	50	[39]
CQDs	Hydrothermal	Branched polyethyleneimine	+3.73	/	375/605	Silver ions and L-cysteine	Fluorescence	2	[48]
CQDs	Hydrothermal	Chlorophyll	+11.6	/	360 460/440	Organophosphorus pesticides	Fluorescence	50	[89]
NCQDs	Solvothermal	1,2-Ethylenediamine	+27.6	36.3%	332/406	Ag^{I} and Fe^{III}	Fluorescence	/	[25]
P-CDs	Pyrolysis	Citric acid, glutathione	+15.4	7.59%	350/460	Copper ion	Fluorescence	35	[45]
C-dots	Pyrolysis	Citric acid, glutathione	+20.3	12.6%	345/488	Heparin	Fluorescence	9.04	[54]
CQDs	Pyrolysis	Spermidine trihydrochloride	+19.5	/	430/542	Hyaluronic acid	Fluorescence	0.09 U/mL	[78]
N-CQDs	Hydrothermal	Dried grass	+30.2	22.8%	360/435	Iodide	Fluorescence	10,000	[55]

electrostatically concentrated in the cell nucleus. Cationic CDs nanoenzymes can interact electrostatically with negatively charged biomolecules or cell surfaces to achieve specific or non-specific binding because of their positive charges on the surface. This combination can enrich the cationic CDs nanoenzyme in the target area, thereby enhancing the imaging signal and improving the sensitivity and resolution of imaging. For example, in fluorescence imaging, it can make the fluorescence signal of the target site stronger and easier to observe and analyze. Li et al. prepared high-QY, long excitation wavelength and good optical stability FNCDs with positive surface charges allowing them to bind to negatively charged nucleoli and chromosomes [56], with an optical excitation wavelength of 466 nm, the FNCD enables non-destructive, long-duration imaging of living cells for monitoring the cell cycle in real time and displaying complete cell divisions (Fig. 7(a)).

Wang et al. investigated PEI-functionalized quantum dots (CDs@PEI) possessing high quantum yield in red fluorescence region, and after PEI modification, at 550 nm excitation, the 2% photo-quantum yield (PLQY) of aqueous CDs solution was increased to 25% in aqueous CDs@PEI solution, as seen in Fig. 7(b), where the center of the red emission was clearly enhanced. Compared to the negative surface charge of pure CDs, the surface of CDs@PEI shows positive, which significantly enhances cellular uptake and improves biofluorescence imaging and makes it possible to have clear cell imaging in the red fluorescent region (Fig. 7(b)). It possesses better photostability than commercial red-emitting dyes [107]. Sun et al. investigated the development of red-emitting CDs for rapid nuclear staining of cells by targeting nuclear proteins. The mechanism for efficient staining is based on the fact that they are small and positively charged, accumulate rapidly in the nucleus, and interact strongly with nuclear proteins at histidine and arginine amino acid residues, resulting in tens of fold enhancement of fluorescence. Moreover, red-emitting CDs do not bind to DNA and do not cause genetic damage [108].

Rohan et al. used the multi fluorescence characteristics of cationic CDs to carry out research on fingerprint data acquisition and analysis (Fig. 8(a)). They used FTIR imaging of cationic CDs in fingerprints to understand the lipid interactions and found that the intensity of fingerprints increased in the presence of cationic CDs. Since CDs are fluoroscopic imaging probes, there is no any reaction or contamination of crime scene evidence, this imaging probe has potential applications in forensics. Also, the cationic CDs do not produce active oxygen, so they can be used safely. Moreover, they can obtain patterned fingerprints with relatively good resolution in a short time, with the ability to study them using a mobile camera, and the fingerprints can be visualized up to the third level, allowing very fast fingerprint detection [41].

In biomedicine, it is desirable to utilize green resources for synthesizing long-wavelength emitting CDs via environment-friendly reactive routes. Zhu et al. prepared green fluorescent N doped CDs (N-CDs) from lotus leaf juice along with ethylenediamine for carbon as well as N sources [109]. With a positive charge, N-CD has two distinctive fluorescence emission peaks and form aggregates with negatively charged $(NaPO_3)_6$ through electrostatic interactions. The fluorescence at 509 nm is burst by $(NaPO_3)_6$ via aggregation-induced burst (AIQ) in the presence of acid phosphatase (ACP), which can hydrolyze $(NaPO_3)_6$ into phosphate fragments and thus disrupt the aggregation of $(NaPO_3)_6$ with carbon dots, as shown in Fig. 8(b). As a result, the burst fluorescence at 509 nm was recovered. Based on this, an efficient ratiometric fluorescent probe can be established to enable intracellular ACP imaging. Hoan et al. hydrothermally synthesized green emitting CDs from lemon juice (Fig. 8(c)), and the PL intensity of CDs increased with increasing hydrothermal time and temperature. Moreover, the CDs diluted with polar solvents are able to induce enhanced luminescence compared to pure CDs. Its strong and stable luminescence properties are especially significant in terms of potential applications in biological imaging [110].

Fang et al. synthesized cationic CDs/Ag composite nanomaterials using arginine as the carbon source and silver ions as the reducing agent, which are more useful in biological imaging because they exhibit fluorescence with emission spacing and red-shift excitation compared to pure CDs. They not only have fluorescence imaging

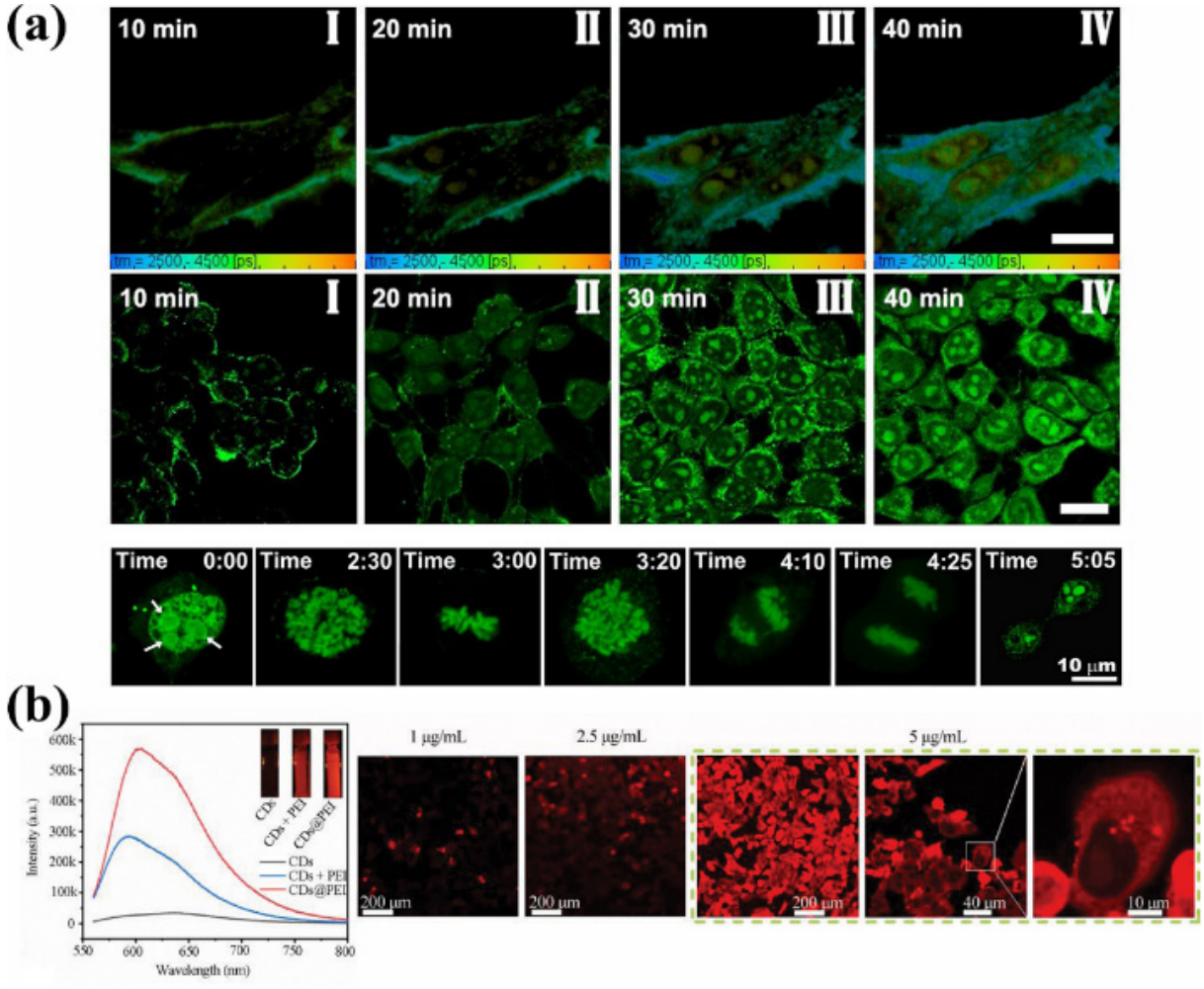

Figure 7 (a) After adding FNCDs, the FLIM and CLSM images of 4T1 cells under different times, and dynamic monitoring of nucleoli and chromosomes by FNCDs during the cell cycle process (prophase, metaphase, anaphase, telophase and interphase) [56]. Reproduced with permission from Ref. [56], © Elsevier B.V. All rights reserved 2020. (b) PL spectra of CDs, CDs@PEI and CDs + PEI dilute aqueous solutions under excitation at 550 nm, and the fluorescence confocal microscope images of stained Hepa1-6 cells upon laser irradiation (543 nm) [107]. Reproduced with permission from Ref. [107], © Published by Elsevier B.V. on behalf of Chinese Chemical Society and Institute of Materia Medica, Chinese Academy of Medical Sciences.

effect on *E. coli* (Fig. 8(d)), but also have stronger bactericidal ability than pure CDs [111]. Here, we summarise the use of cationic CDs in imaging in Table 2.

(2) Targeted imaging: Through reasonable design, cationic CDs nanoenzymes can be combined with specific targeting molecules to construct targeted imaging probes. The positive charge of the electropositive CDs nanoenzyme is helpful for the stable combination of the electropositive CDs nanoenzyme and a target molecule, and the electropositive carbon-dot nanoenzyme can actively target specific pathological cells or tissues, such as tumor cells, *in vivo*. After reaching the target site, the imaging function, such as photoacoustic imaging and magnetic resonance imaging, can be used to achieve accurate imaging of the lesion site, providing strong support for early diagnosis and localization of the disease [112].

(3) Imaging-guided therapy monitoring: In the course of therapy, cationic CDs nanoenzymes can be used as both imaging agents and therapeutic agents or therapeutic adjuvants. Its imaging function can be used to monitor the distribution and metabolism of drugs and the changes of diseased tissues in real time during treatment. For example, in photothermal therapy or photodynamic therapy, the imaging characteristics of cationic CDs nanoenzyme can help doctors accurately judge the therapeutic effect and adjust the treatment plan in time [113].

CDs nanoenzyme combines the catalytic ability of nanoenzyme and imaging technology, which is expected to realize the integration of diagnosis and treatment, and has a wide application prospect in the biomedical field.

3.2.2 *Antibiosis*

Among various antimicrobial nanomaterials, CDs can cause interaction with bacterial cells due to their structure and surface molecular design, and CDs with positively charged surfaces through macromolecular modifications can have a strong antimicrobial ability against bacteria. The antimicrobial mechanism of CDs is generally the gene busting effect of CDs or oxidative stress associated to reactive oxygen species (ROS) formed by means of the introduction of hydrogen peroxide [114, 115] or light irradiation [116–119]. Travlou et al. demonstrated that the antimicrobial activity of N-doped CDs would be far above that of S-doped CDs (Fig. 9(a)). The advantage of general nitrogen functional groups is reflected in an amine and amide protonated form, where they can

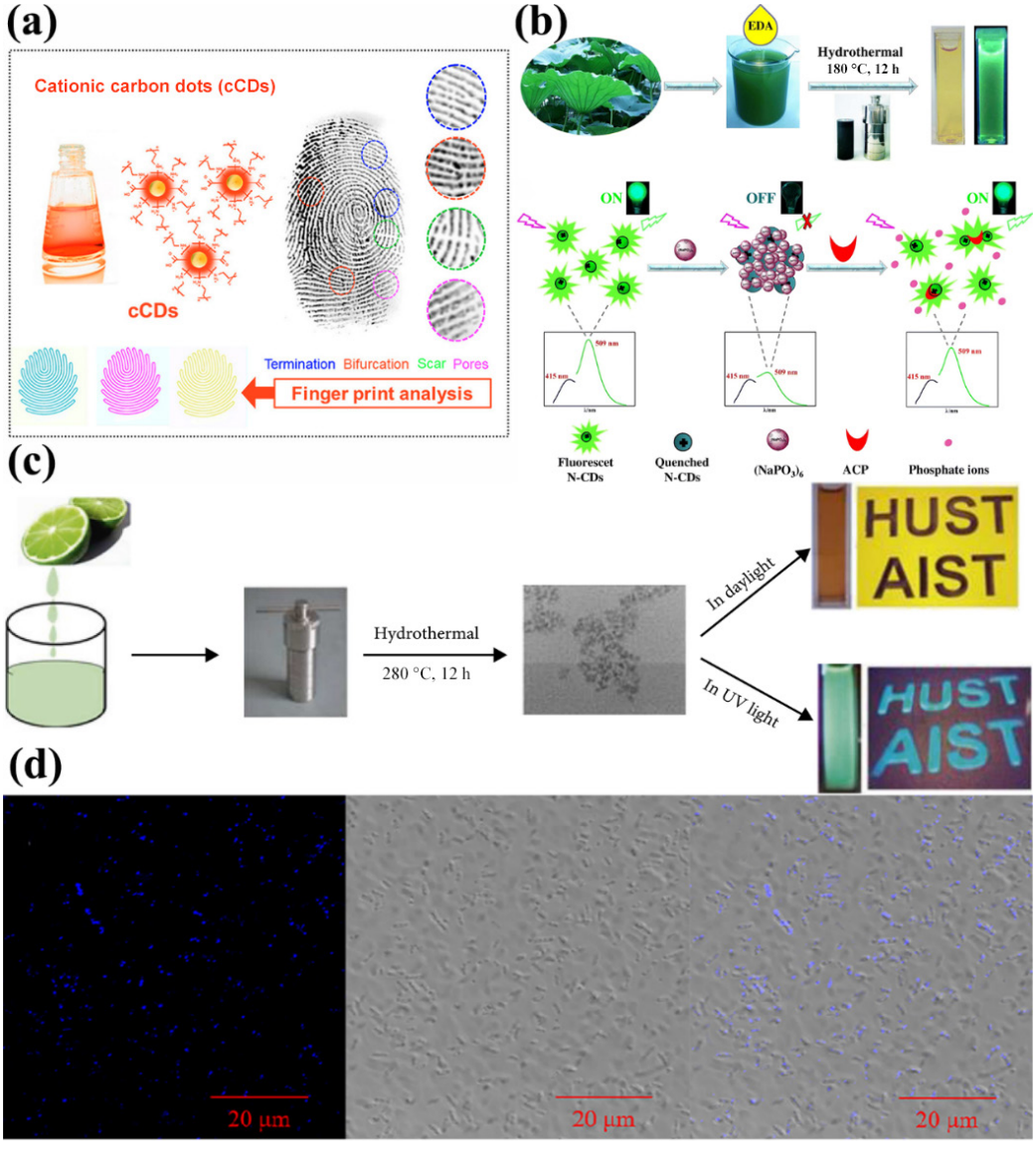

Figure 8 Schematic illustration of (a) cationic CDs for solid-state fingerprinting [41]. Reproduced with permission from Ref. [41], © Published by Elsevier B.V. 2018. (b) The preparation of N-CDs from lotus leaf and the design and principle for ACP detection based on the AIQ and enzymolysis approach [109]. Reproduced with permission from Ref. [109], © Springer-Verlag GmbH Austria, part of Springer Nature 2019. (c) Hydrothermal process of lemon juice for synthesis of C-dots and characters building from CDs [110]. Reproduced with permission from Ref. [110], © Bui Thi Hoan et al. 2019. (d) Confocal images of *E. coli* in the presence of CDs/Ag composite nanoparticles under the irradiation of 405 nm laser and white light as well as the merged image [111]. Reproduced with permission from Ref. [111], © IOP Publishing Ltd 2019.

Table 2 The application of cationic CDs in imaging

Cationic CDs	Synthesis approach	Precursors	Zeta potential (mV)	Ex/Em (nm)	Analytes	Imaging mode	Ref.
cCDs	Microwave	Citric acid	+6.64 ± 0.53	375/605	Fingerprint	Fluorescence	[41]
FNCDs	Hydrothermal	Glycine	+6	488/640	Probes	Fluorescence	[56]
CDs@PEI	Microwave	Citric acid, urea	+8.936	450/550	Bioimaging	Fluorescence	[107]
N-CDs	Hydrothermal	Lotus leaf juice, ethylenediamine	+2.93 ± 0.30	415/509	Acid phosphatase	Fluorescence	[109]
C-dots	Hydrothermal	Lemon juice	+18.8	400–480/500–550	Bioimaging	Fluorescence	[110]
C-dot/Ag	Hydrothermal	L-arginine	+3.22	370/455	Gram-negative bacteria	Fluorescence	[111]

react with bacteria cell membranes that are negatively charged. In contrast, although sulfur-containing CDs may depend on mercaptans to exert antimicrobial effects, their antimicrobial effect is relatively weak because dissociation of carboxyl, sulfonic acid and sulfate groups can make them negatively charged [120].

Zhao et al. reported an N-doped CQDs (NCQDs) with GSH as an antioxidant, and the reduction of sulfhydryl groups by GSH enhanced the antibacterial effect of NCQDs (Fig. 9(b)). It was also shown no ROS was produced by NCQD or mixtures between NCQD and GSH in the fight against bacteria. NCQDs with a

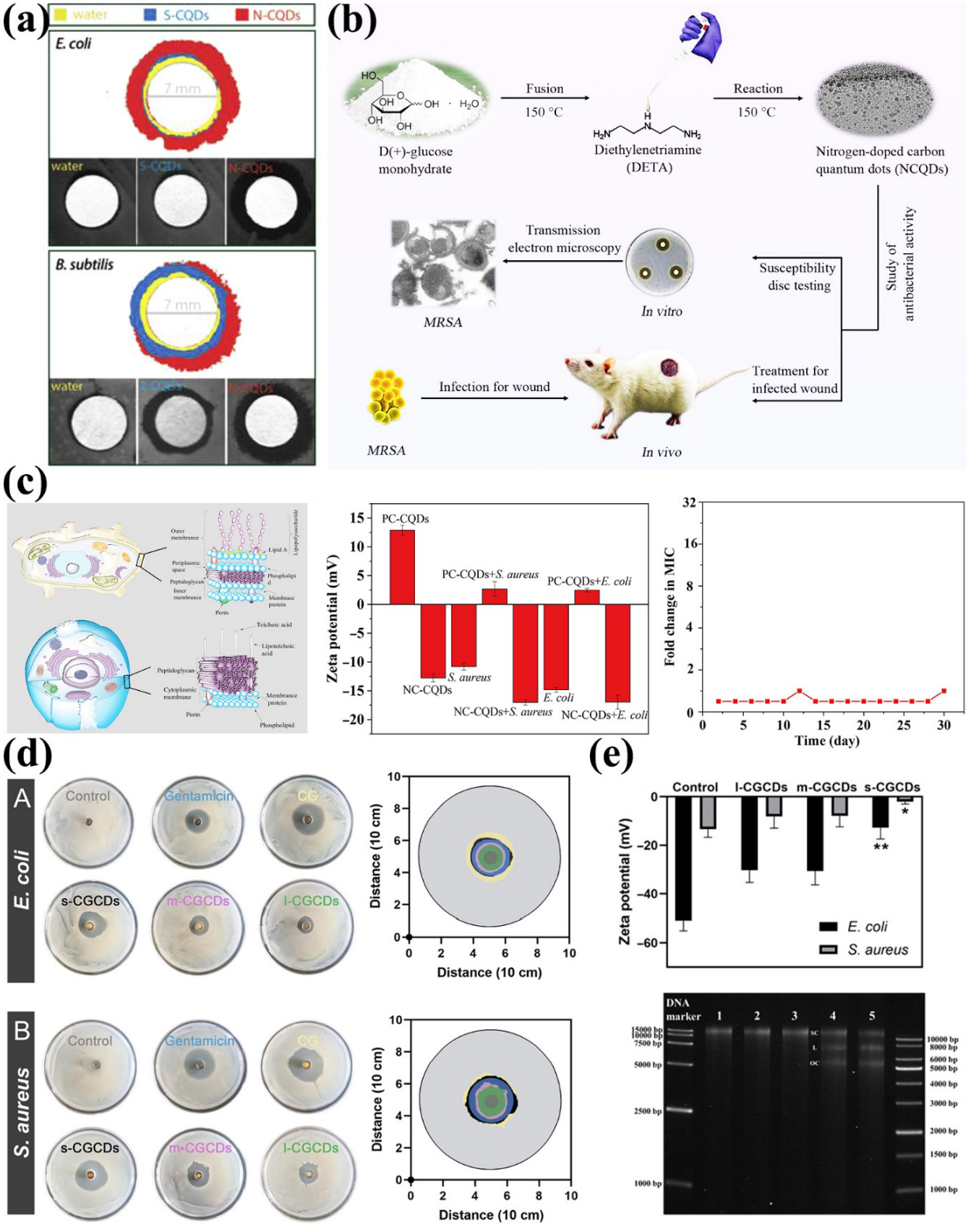

Figure 9 (a) Diffusion discs assay showing the antibacterial activity of the S-CQDs and N-CQDs against *E. coli* (Gram-negative) and *B. subtilis* (Gram-positive) bacteria [120]. Reproduced with permission from Ref. [120], © Elsevier Ltd. All rights reserved 2018. (b) Synthesis and antibacterial properties of NCQDs and their therapeutic effect on wounds infected with MRSA [121]. Reproduced with permission from Ref. [121], © Published by Elsevier B.V. 2019. (c) The schematic diagram of the cell wall structure of *S. aureus* and *E. coli*, Zeta-potential and resistance acquisition of *S. aureus*, *E. coli*, and MRSA during continuous exposure to PC-CQDs [122]. Reproduced with permission from Ref. [122], © Elsevier B.V. All rights reserved 2021. (d) Inhibition zone photos of the control group, gentamicin (40 lg/mL), CG (400 lg/mL), s-CGCDs (400 lg/mL), m-CGCDs (400 lg/mL), and l-CGCDs (400 lg/mL) against *E. coli* and *S. aureus* (3 × 107 CFU/mL) on MHA medium for 24 h and schematic diagram of the inhibition zone area [57]. (e) Zeta potentials and Gel electrophoretic images of plasmid DNA (from *E. coli*) treated with s-CGCDs, m-CGCDs, and l-CGCDs [57, 115]. Reproduced with permission from Ref. [57], © Elsevier Inc. All rights reserved 2020.

positive charge have a special antimicrobial activity against staphylococci, where it first engages in interaction with negatively charged bacteria before being anchored to certain specialized sites on the staphylococcal surface. The plasma membrane of *S. aureus* and its related bacteria is distributed with a thick layer of interlinked peptidoglycan, so cell walls are porous. And the porous cell wall can facilitate the interaction between NCQDs and *S. aureus* and methicillin-resistant *S. aureus* MRSA, and thus exert bactericidal effects. They also investigated the *in vivo* therapeutic effects of NCQDs on infected wounds and their cytotoxicity to mammals. The results showed that NCQDs were as effective as vancomycin in the treatment of MRSA-infected wounds, NCQDs were no toxic side effects to the organism [121].

Hao et al. designed N-doped CQDs (PC-CQDs) with positive charge based on citric acid carbon source [122]. PC-CQDs are enriched by electrostatically interacting with negatively charged bacteria and then interfering with their genes and producing reactive oxygen species, which can lead to bacterial rupture. Moreover, PC-CQDs interacted with *S. aureus*, *E. coli* and MRSA for thirty days without inducing the evolution of drug resistance, while it showed identical therapeutic efficacy with levofloxacin hydrochloride in a wound model of mixed *Staphylococcus aureus* and *Escherichia coli* infections. They also found that PC-CQDs were more efficient in inhibiting Gram-positive bacteria than Gram-negative bacteria. Although PC-CQDs can attach to bacteria cells through electrostatic interaction, compared with Gram-negative bacteria, which have a dense yet thinner cell wall structure, Gram-positive bacteria have a lax and thicker membrane structure that is better suited for the uptake of PC-CQDs (Fig. 9(c)).

Shen et al. investigated the effect of different particle sizes of CQDs i.e. ~ 2.0 nm small particle size (s-CGCDs), ~ 3.9 nm medium particle size (mCGCDs) and ~ 5.3 nm large particle size (l-CGCDs) on antibacterial activity. They have the same precursors and therefore have the same properties, but they show differences in terms of bacterial inhibition (Fig. 9(d)) [57]. l-CGCDs are extremely stable in physiological environments by inheriting the highly positively charged properties of their precursors. There is no generation of intracellular ROS in the antimicrobial process. They evaluated the three CGCDs using Gram-negative *E. coli* and Gram-positive *S. aureus*. s-CGCDs inhibited *Escherichia coli* with a diameter of ~ 25.88 mm and *Staphylococcus aureus* with a diameter of ~ 30.68 mm, which is significantly larger than the inhibition diameter of the other two particle sizes of CGCDs, indicating it has the highest antibacterial activity. As shown in the Fig. 9(e), after treatment with s-CGCDs, the ratio of SC conformers dropped whereas the ratios of L and OC conformers increased, indicating s-CGCDs can unravel double-helical structures. After 1H nuclear magnetic resonance (NMR) spectroscopy, small-sized DNA showed a greater degree of deuterization and lower spatial site resistance, which enabled the official group full access to the DNA molecule, and thus relaxed its structure.

Yu et al. synthesised antibacterial and anti-inflammatory bifunctional carbon dots, AAB-CD, with ultra-small size (2.3 nm), abundant surface functional groups, high Zeta potential (30.9 mV) and excellent biocompatibility. The carbon dots have excellent antimicrobial properties to reduce the risk of bacterial resistance, while the rich surface functional groups impart stable antioxidant properties for sustained wound anti-inflammation. It can be used as the main active material in the manufacture of hydrogel wound dressings to promote wound healing [35].

3.2.3 *Therapy*

Currently, cationic CDs have promising applications mainly in cancer, infections and gene therapy.

Pan et al. studied the design of positively charged CD/WS2 heterojunctions. Compared with pure CD or WS2, CD/WS2 heterojunctions exhibit collaboratively increased light absorbance as well as higher overall photothermal transfer efficiencies in the near-infrared second window (NIR-II). The heterogeneous junction and the significantly larger size considerably enhance the targeted ability within the tumorous tissue of the NIR-II responsive CD component via IV injection, resulting in total tumoral regression with fairly low intensity of laser irradiation (0.6 W/cm^2 at 1064 nm) (Fig. 10(a)). Meanwhile, the heterogeneous ligation greatly increased the physiologic stabilities and did not show any clumping in PBS and blood. Moreover, its mild photothermal effect significantly enhanced osteogenic differentiation (Fig. 10(b)) and significantly upregulated the expression of bone-related genes, especially heat shock proteins, which make it possible to use it for the treatment of osteosarcoma [58].

Feng et al. investigated a carrier containing charge-convertible CDs on the basis of cisplatin(IV) prodrug loading, which was prepared by the covalent functionalization of CDs (CDs-Pt(IV)) complexes with PEG-(PAH/DMMA) and cisplatin(IV) prodrugs via electrostatic interactions (Fig. 10(c)). Due to the presence of charge conversion properties in the extracellular microenvironment of tumor cells, this carbon dot carrier enhances the internalization of tumor cells compared to carriers without charge conversion properties [123]. Under normal physiological conditions, it has fewer side effects and cisplatin(IV) prodrugs in the reducing cellular fluid of cancer cells can control the release of toxic anticancer drugs (Fig. 10(d)).

Barras et al. showed that positively charged CQDs can disrupt ocular vitreous collagen fibrillation and prevent type I collagen fibrillation, and at low energy levels this can successfully disrupt vitreous turbidity in ocular patient samples (Fig. 10(e)). The mechanisms by which CQDs inhibit collagen fibrillation include electrostatic and hydrophobic interactions between neighbouring molecules and heat absorption reactions. Usually, hydrogen bonding is considered to be the most stable force in these proteins. So, they speculated that the CQDs they prepared with carbon and carboxyl groups on the surface might form hydrogen bonds with amino and hydrogen groups in the collagen type I protein. It may change interaction force among collagen molecules. Among other things, size and surface charge have been suggested to be key factors in their anti-fibrotic properties. Negatively charged CQD decreases the interaction with collagen fibers. They tested the effect of destruction after orthoelectric CQD treatment and pulsed laser irradiation in terms of the true clouding of the vitreous in patients after vitrectomy. A significant reduction in turbidity was noted following 50 pulses (561 nm; 4.5 J/cm^2) while the glassy samples mixed together with the CQD (Fig. 10(f)). This dual effect could allow further exploration of CQD in the context of fibrotic diseases, even those involving protein aggregation [124].

Lei et al. developed an intranasal vaccine comprising cationic crosslinked carbon dots (CCD) and the SARS-CoV-2 antigen RBD-HR, which spontaneously forms antigenic particles. Administration of this CCD/RBD-HR vaccine through the nose stimulates the production of high levels of antibodies capable of broadly neutralizing authentic viruses and pseudoviruses, including Omicron and its variants. The findings suggest that CCD holds

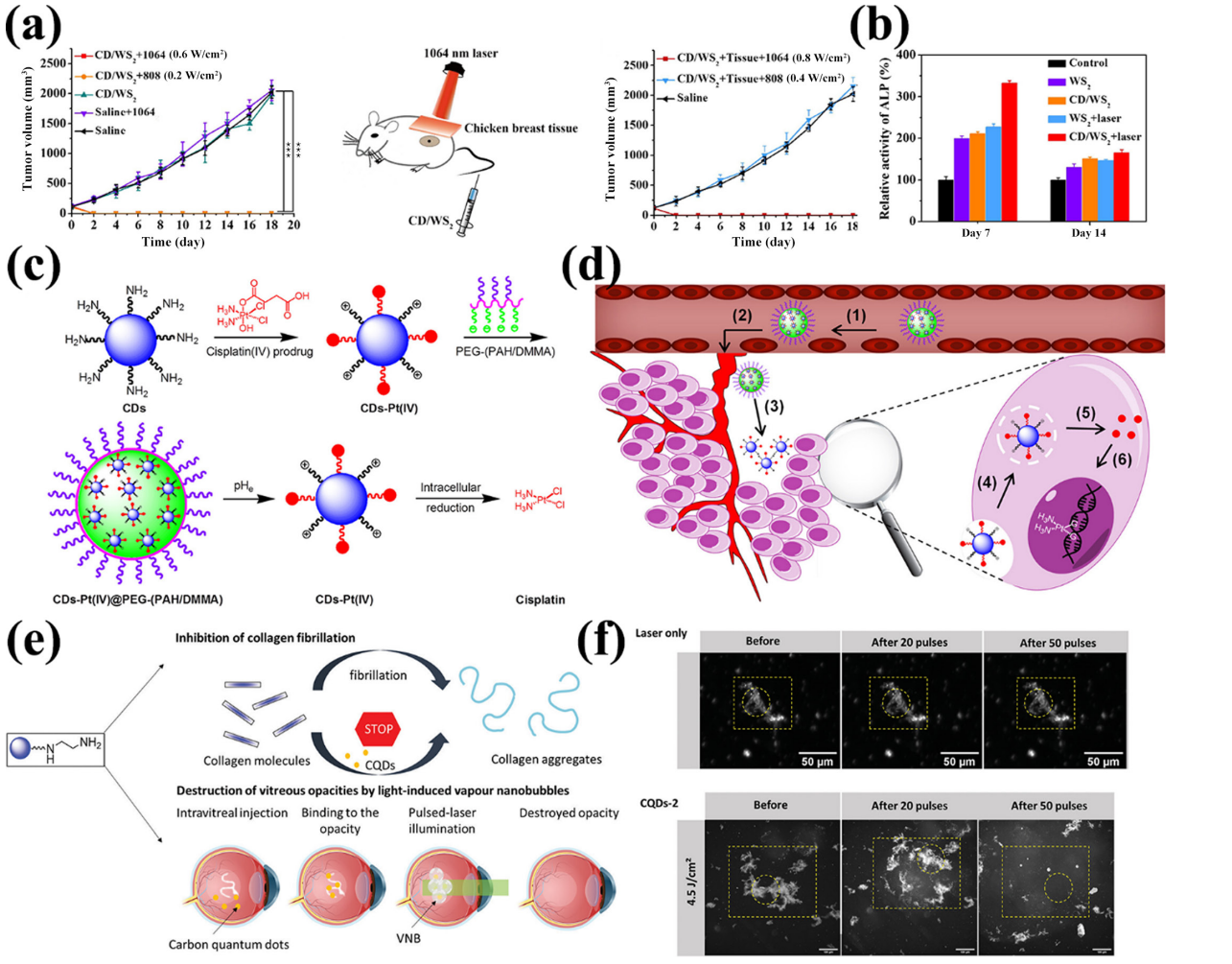

Figure 10 (a) Tumor growth curves of mice after receiving different treatments via intravenous injection, schematic illustration of deep tissue PTT, and tumor growth curves of mice after receiving different deep tissue PTT treatments via intravenous injection. (b) Effects of different samples on the ALP activity of osteoblasts [58]. Reproduced with permission from Ref. [58], © Elsevier B.V. All rights reserved 2019. (c) Schematic illustration for the preparation of charge-convertible CDs-based drug nanocarrier CDs-Pt(IV)@PEG-(PAH/DMMA). (d) Schematic illustration for the drug delivery process of CDs-Pt(IV)@PEG-(PAH/DMMA) [123]. Reproduced with permission from Ref. [123], © American Chemical Society 2016. (e) CQDs to inhibit the formation of collagen aggregates (top) and to destroy collagen aggregates by light induced VNBs (bottom). (f) Dark-field microscopy images of human vitreous opacities [124]. Reproduced with permission from Ref. [124], © The Royal Society of Chemistry 2021.

promise as an intranasal vaccine adjuvant for enhancing mucosal immunity and could potentially serve as an adjuvant candidate for the development of intranasal vaccines against various infectious diseases, such as COVID-19 [125].

3.2.4 *Non-viral gene carriers*

Although bioimaging and gene therapy are promising, there are still many challenges. It is the major difficulty to search for appropriate materials to image or deliver the genetical material (DNA, RNA, small interfering RNA, microRNA) into targeted cells [126–130]. To realize the goal for gene treatment, efforts have been made to development of gene vectors, and these vectors can be roughly classified in two categories: viral vectors and non-viral vectors [131, 132]. Non-viral gene vectors are expected to be efficient vectors for transfection, but problems of immunogenicity, carcinogenicity as well as inflammation have raised severe worries about their clinical application. The main requirements for the clinical application of these materials include low toxicity, cellular targeting and high transfection efficiency [133].

Since conventional quantum dots are made of heavy elements including Pb, Se, cadmium sulfide and cadmium selenide, they have relatively poor biocompatibility and high toxicity [134–136]. Moreover, most non-viral gene carriers (e.g., calcium phosphate nanoparticles [137] and cationic polymers [138]) have not been characterized as self-imaging properties so far. Thus, using CQDs may replace conventional semiconductor quantum dots with noxious heavy metals. They can also be developed with appropriate modifications to have positive surface charge and become self-tracking drug/gene carriers.

Zhou et al. synthesized cationic CDs by a green and low-cost process using sodium alginate as a carbon source [48]. The average fluorescence quantum yield (FLQY) of the prepared CQDs was 12.7%. Aqueous solutions of CQDs emitted blue fluorescence. Meanwhile, CQDs have strong plasmid DNA concentration ability, low toxicity, high transfection efficiency and good biocompatibility, they can be used to transport plasmid transforming growth factor-β1 (TGF-β1) to 3T6 cells by gene carriers or to detect protein delivery process as probes to elucidate the mechanism of cytosolic

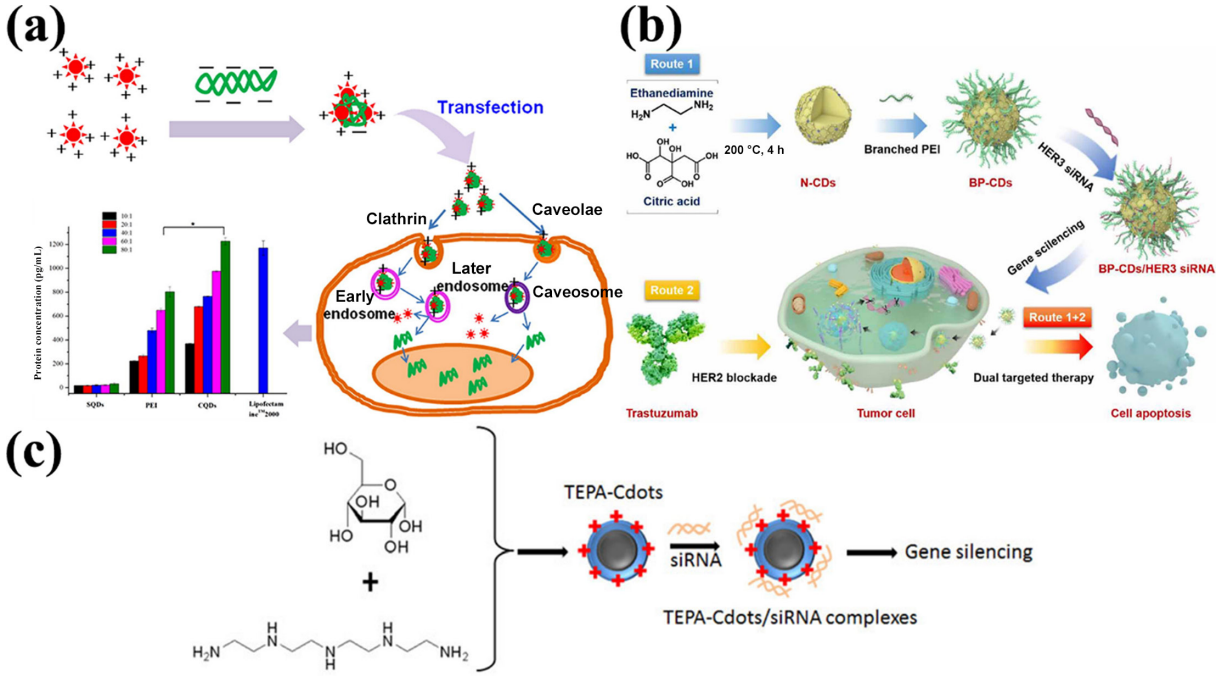

Figure 11 (a) Schematic diagram of alginate-derived photoluminescent CQDs as non-viral gene vectors, and the transfection efficiency of CQDs/pDNA complexes *in vitro* gene [48]. Reproduced with permission from Ref. [48], © Acta Materialia Inc. Published by Elsevier Ltd. All rights reserved 2016. (b) The dual targeted therapy in HER2-positive breast cancer cells with the combination of BP-CDs/HER3 siRNA and Trastuzumab [139]. Reproduced with permission from Ref. [139], © IOP Publishing Ltd 2020. (c) TEPA-C dots preparation, TEPA-C dots/siRNA complexes formation and its gene silencing effect [141]. Reproduced with permission from Ref. [141], © Taylor & Francis Group, LLC 2019.

uptake for CQDs and pDNA complex. Enzyme blotting immunosorbent assay (ELISA) coupled with laser confocal scanning microscopy were utilized to assess the effects of genetic transfection as well as inhibition of cellular uptake (Fig. 11(a)). This findings showed that the cation CDs could play roles as both non-viral gene vectors and bioimaging probes.

PEI, one of the most studied non-viral gene vectors, can efficiently transfect to mediate gene delivery without causing enzymatic degradation, but it has strong cytotoxicity. While Shu et al. investigated a PEI functionalized N-doped CDs (BP-CDs), the presence of which effectively reduced cytotoxicity and could successfully deliver enhanced green fluorescent protein genes into Cos-7 cells, and further investigated the BP-CDs/HER3 siRNA complex (Fig. 11(b)). BP-CD's stable interaction with human epidermal growth factor receptor 3 (HER3) siRNA protects HER3 siRNA against biodegradation as well as improves its transfection efficiency. Treatments with BP-CD/HER3siRNA compounds alone or combined with trastuzumab showed excellent therapeutic effects in suppressing the cell reproduction of BT-474 cells [139]. Manuel et al. used a combination of PEI-coated CDs to easily generate cationic CDs by electrostatic binding, enabling sophisticated transfection protocols to generate retroviral vectors by co-transfecting three different plasmids into packaging cells, demonstrating not only high efficiency but also functionality for gene delivery and testing the ability to generate infectious retroviral particles [140].

Wang et al. synthesized a novel CDs (TEPA-CDs) by a bottom-up approach using glucose and tetraethylene pentamine (Fig. 11(c)). TEPA-CDs have a Zeta potential of 19.17 ± 1.33 mV and can concentrate siRNA into stable complexes, and they assessed cellular uptake of TEPA-CD/siRNA complexes using cy3-labeled siRNAs. HeLa cell fluorescence was examined via the confocal laser scanning microscope (CLSM) method, with red fluorescence located primarily in the vicinity of the nucleus in a diffuse distribution. This result indicates that cy3-labeled siRNA was successfully transfected into TEPA-CDs-mediated HeLa cells. The TEPA-CDs/siRNA complex significantly inhibited the expression of green fluorescent protein (GFP) in HeLa-EGFP cells [141]. This indicated that these TEPA-CDs could be used as a siRNA nanocarrier to tumor cells.

Chen et al. demonstrated that conjugating cationic carbon dots with a lipid structure like oleic acid (OA) significantly enhanced gene transfection efficiency. In their study, they created a type of cationic carbon dot, termed APCDs, using arginine (Arg) and pentaethylenehexamine (PEHA) as precursors, and subsequently conjugated them with OA. By adjusting the mass ratio of APCDs to OA, they synthesized three conjugates: APCDs-0.5OA, APCDs-1.0OA, and APCDs-1.5OA. Upon internalization by HEK 293 and osteosarcoma (U2OS) cells, the conjugates distributed within both the cytoplasm and the nucleus. When utilized as gene delivery vehicles, the APCDs-OA conjugates successfully transported plasmid DNA (pDNA) encoding the green fluorescence protein (GFP) gene into both HEK 293 and U2OS cells. Notably, the GFP expression levels facilitated by APCDs-0.5OA and APCDs-1.0OA were ten times higher than those achieved with PEI in HEK 293 cells. Additionally, APCDs-0.5OA showed remarkable siRNA transfection efficiency, evidenced by the significant downregulation of recombinant human Fanconi anemia group A protein (FANCA) and Fanconi anemia group D2 protein (FANCD2) expression after delivery of FANCA siRNA and FANCD2 siRNA into U2OS cells [142].

In addition to these applications, CDs can also interact with human serum albumin (HSA) in biomedical applications. HSA is one of the most important serum proteins and its main

physiological function is to maintain blood osmolarity homeostasis and to be involved in transportation and metabolization of various drugs including even exterior nanomaterials. It has unique functions and medicinal significance in the circulatory system, so it is considered as one of the most significant model proteins [143, 144]. A comprehensive study of the effect of CDs size, surface functional groups and core structure on the interaction with HSA is more important and necessary. Li et al. used polyethylene glycol (PEG) and PEI for surface modification of pure CDs to obtain negatively charged PEG CDs and positively charged PEI CDs. They were investigated by various photophysical, electrochemical and calorimetric measurements that both CDs can effectively bind HSA, and HSA and PEI CDs are associated with each other by electrostatic forces, while PEG CDs are associated with HSA by hydrophobic and van der Waals forces. Both carbons quench the strong fluorescence from the Trp residue in HSA in a charge-independent way. They used Hill's equation and electrochemical impedance spectroscopy (EIS) to demonstrate how the binding constants of CD and HSA to each other are minimally influenced by varying surface charges. Three-dimensional fluorescence spectra show that negatively charged CDs do not perturb the secondary structure of HSA, whereas higher concentrations of CDs significantly alter the secondary structure of HSA when compared to low concentrations of PEI CDs [145].

In the biomedical field, the small size and easy functionalization of cationic CDs enable them to cross natural biological barriers in the body, such as the blood-brain barrier and the glomerular barrier. Meanwhile, their high fluorescence quantum yield and long emission lifetime give cationic CDs great potential for bioimaging, which can be used for cellular fluorescence imaging, *in vivo* fluorescence imaging in animals and tumour diagnosis. They can interact with negatively charged biomolecules (such as DNA and proteins) through electrostatic interaction, and can be used as drug carriers for drug delivery to achieve localization and targeted delivery to specific cells or tissues, improving the therapeutic effect of drugs and reducing side effects. In addition to their use as drug carriers, cationic CDs can also be used in photodynamic therapy by absorbing specific wavelengths of light and generating excited states, which has a better therapeutic effect on tumors and other diseases.

3.3 Catalysis

Natural enzymes are powerful biocatalysts that have found applications in various fields, including industry, medicine, and biology. However, their practical use is often hindered by inherent drawbacks such as low stability and high costs associated with their preparation and purification. To address these issues, various nanomaterials have garnered considerable attention due to their stable structures, lower costs, and adjustable activity [146–148]. A large amount of research has focused on the development of advanced carbon nanomaterials as green and sustainable catalysts for energy conversion [149–154]. Among these, CDs have emerged as a significant research focus in the biomedical field, thanks to their excellent water solubility, biocompatibility, and diverse functional groups. Commonly regarded as an ideal substitute for molecular dyes and semiconducting particles [155, 156], cation CDs enzyme-like materials can be used as photosensitizers in photocatalytic processes. Bonding of CDs to semiconductors (TiO_2, CoO, Cu_2O, Fe_2O_3,...) can enhance their photocatalytic activity and electrical conductivity [157, 158]. Antonino et al. showed spontaneous electrostatic coupling between cationic CDs with Dawson type polyoxymethylene (POM) ($[P_2W_{18}O_{62}]^{6-}$). The presence of efficient electron transfer in CDs-POM mixtures was demonstrated using ultrafast transient spectroscopy, which leads to the formation of charge-separated states within 120 fs of light absorption. In addition, they investigated the photoreduction of silver ions by CDs-POM. The reduction of silver ions all appeared as a plasma band at around 420 nm, and its intensity increased with time. In comparison to (P_2W_{18}), blueshift of the plasma band indicates that it forms smaller nanoparticles. They also demonstrated the way in which CDs serve as electronic repeaters to improve the catalytic performance for several POM, while summarizing the mechanisms of the different steps of silver ion reduction from CDs/(P_2W_{18}) under visible light illumination (Fig. 12(a)). This new CDs-POM mixture can reduce and recover precious heavy metals and reduce protons into hydrogen for use in water pollution processes. Moreover, reactions involving metal reduction can be coupled with organic pollutant degradation as an alternative to sacrifice electron donors [159–161].

Mateusz et al. reported the electrocatalytic properties of positively charged carbon nanomaterials for the electrooxidation of flowing ascorbic acid. The presence of positively charged nanomaterials enhances the signal generated by electrooxidation and the magnitude of the signal is related to the collective effect of positively charged carbon nanomaterials and their adsorption, and the adsorption of the important fraction is irreversible. The electrostatic interaction between positively charged carbon nanomaterials and ascorbic acid anion also affects the electrochemical signal, this signal is dependent on the concentration of positively charged carbon nanomaterials and multiplication injections can increase the sensitivity [162]. Gan et al. prepared chain-like Au/CDs (GCDs) nanocomposites by electrostatic self-assembly of cationic CDs and negatively charged Au nanoparticles. Cross-linking reactions occur between amino and carboxyl groups on the CDs surface resulting in the formation of chained Au aggregates enclosed in carbon shells. The Au aggregates can boost the electromagnetic field and thus enhance the signal of surface-enhanced Raman scattering (SERS), and the electron transfer between CDs and Au makes the nanocomposites highly catalytic. GCDs can be used for catalyzing colorless 3,3',5,5'-tetramethylbenzidine (TMB) oxidation into blue oxTMB when hydrogen peroxide is present, which shows stronger peroxidase-like activities than Au nanomaterials or CDs alone (Fig. 12(b)). Also, GCDs can be further used for enzyme mimics to detect glucose [163].

In addition, numerous studies have reported that CDs exhibit peroxidase, catalase, superoxide dismutase, and glutathione peroxidase activities. CDs can be doped with metal elements to adjust the surface chemical properties and electronic structure, and then obtain excellent peroxidase-like activity. For example, Cu-doped CDs can effectively catalyze the decomposition of H_2O_2 to produce hydroxyl radicals with strong oxidizing properties, showing peroxidase-like activity [164]. O/N-CDs prepared from polyaniline precursor have peroxidase-like activity and can be converted to catalase-like activity under illumination, and both activities can be accurately controlled by light intensity. CDs exhibiting catalase activity are able to scavenge H_2O_2 from the body, thereby protecting cells from oxidative damage. This property makes CDs potentially useful in antioxidant therapy [165]. Some studies have shown that CDs can scavenge superoxide anion free radicals to a certain extent, play a role similar to superoxide

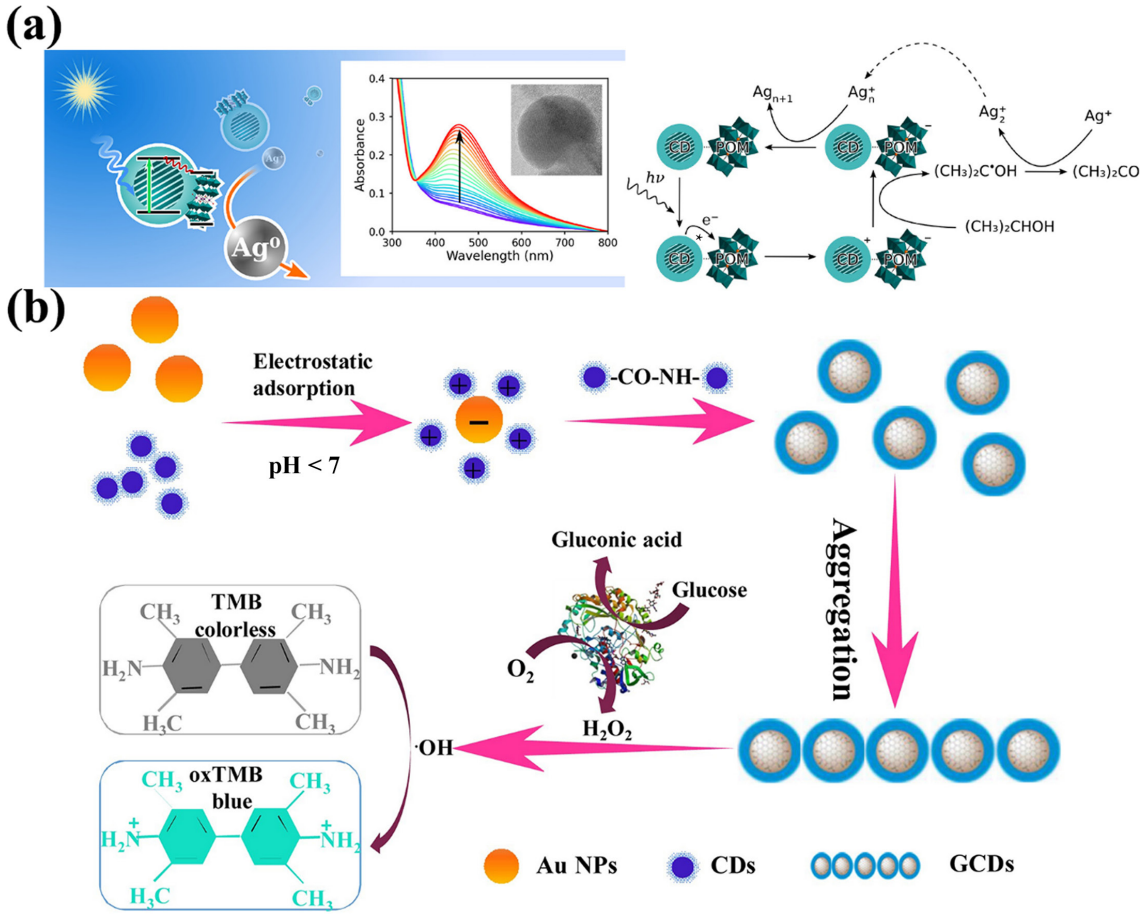

Figure 12 (a) UV–vis absorption spectra measured under visible illumination of a deaerated aqueous solution and proposed mechanism explaining the reduction of silver ions from CDs/(P_2W_{18}) under visible illumination [159]. Reproduced with permission from Ref. [159], © Published by Elsevier Ltd 2021. (b) A schematic illustration for the synthesis of GCDs nanocomposites and the colorimetric detection of glucose based their peroxidase mimetic properties [163]. Reproduced with permission from Ref. [163], © Elsevier B.V. All rights reserved 2021.

dismutase, help to maintain the stability of cellular homeostasis and reduce oxidative stress damage. The nano-enzyme has the advantages of high stability, easy preparation, low cost, easy large-scale production and the like [166]. Some surface-modified CDs can participate in the reduction reaction of glutathione and play a role in catalyzing the decomposition of H_2O_2 and organic peroxides, similar to the function of glutathione peroxidase, which helps to protect cells from oxidative damage and maintain the balance of redox state in cells.

In catalytic applications, cationic CDs show good catalytic activity. Their large specific surface area and abundant surface functional groups provide more catalytically active sites. Additionally, the tunable functional properties of cationic CDs make them excellent nanocatalysts or catalyst supports, suitable for developing new catalytic processes, such as organic transformations and artificial photosynthesis. Their catalytic activity in peroxidase, catalase and other species highlights their potential applications in the field of detection and treatment of bacterial infections.

4 Summary and perspectives

The emergence and flourishing development of cationic CDs as enzyme-like materials have addressed several limitations of natural enzymes, including low operational stability, high costs, extended purification times, and difficult storage. In this review, we provide an overview of the synthesis strategies and the physical and chemical properties of enzyme-like cationic CDs. Furthermore, we detail their applications in sensing, biomedicine, and catalysis. Despite the significant progress made in the design, synthesis, and application of mimetic enzymes using cationic CDs, there are still challenges and obstacles that need to be addressed in future research.

(1) Recent reports suggest that cationic CDs can serve as effective imaging nano-enzymes. However, there are limited studies on how altering the surface charge of CDs can significantly enhance their red emission when dispersed in aqueous solutions. Developing CDs with optimal cellular uptake that also exhibit efficient red emission in water presents a significant challenge for improving bioimaging techniques and therapeutic applications. Systematic studies on the interaction, localization and antagonism of cationic CDs against bacteria, as well as the assessment of the potential for further antimicrobial evolutions to take place in antimicrobial CD is still lacking. Therefore, it is a challenging and necessary task to understand interactions and inhibition mechanisms of CDs that possess wide-spectrum antimicrobial ability with reduced minimal inhibitory concentrations that do not induce resistances. Cationic CDs have good photostability and can be used as photosensitizers in photocatalytic processes, but their applications in photocatalysis have not been explored in depth yet. The photosensitization effect resulting from the transfer of electrons by the excited CDs with the photocatalyst have not been demonstrated.

(2) The challenges facing nanoenzyme-mimicking cationic CDs in applications include insufficient catalytic activity and incomplete understanding of the catalytic mechanism. Firstly, catalytic activity is one of the key indicators for evaluating the performance of nanoenzymes. However, the catalytic activity of many current cationic carbon dot nanoenzymes is still lower than that of natural enzymes, which limits their application in certain high-precision catalytic reactions. To improve catalytic activity, researchers can dope the carbon dots by trying different doping strategies, such as introducing metal ions and non-metallic elements, to change their electronic structure and chemical activity and increase the number and activity of active sites. Composite structures can also be constructed by combining cationic carbon dots with other catalytically active materials or enzymes to create synergistic effects and improve catalytic efficiency. In addition, the incomplete understanding of the catalytic mechanism is also a factor limiting the application of cationic carbon dot nanoenzymes. Since the catalytic behaviour of nanoenzymes is often more complex than that of natural enzymes, it is difficult to accurately identify their active sites and catalytic pathways. To investigate the catalytic mechanism of nanoenzymes in depth, researchers can use advanced characterisation techniques and computational methods, such as *in situ* spectroscopy and molecular dynamics simulation, to reveal the structural and kinetic changes of nanoenzymes during the catalytic process.

According to the abstract of information from recent reports, we make the below recommendations for future research perspectives in cationic CDs field. We believe that PEI surface modification strategies are potentially applicable to additional long-wavelength emissions, thus facilitating their widespread application in biological imaging and biomedically relevant fields. Biomass-derived CDs are environmentally friendly and easy to recover, usually rich in functional groups, and can easily bind to metal ions. Developing the use of biomass CDs to detect metal ions can solve the problems of complicated operation and expensive equipment of traditional detection methods. Meanwhile, metal nanoparticles can be assembled into composite nanomaterials by cross-linking reaction or electrostatic interaction on the surface of cationic CDs, which can offer additional active sites, increase electronic transport efficiencies, and can be further improved for catalytic applications.

In summary, this review aims to analyze recent progress of cationic CDs, both in terms of diverse synthetic strategies and application areas. Particularly, heteroatom doping and surface functionalization have been shown to be one of the prospective methods in improving the surface charges of CDs by tuning their surface functional groups, dimensions, etc. Hence, we have discussed the excellent properties of cationic CD in fluorescence sensing, biomedicine, catalysis, physisorption and separation in detail. We are convinced that with constant endeavors, cationic CD is going to play an even more significant role in our lives very soon.

Data availability

Not applicable.

Acknowledgements

This work was supported by the National Natural Science Foundation of China (Nos. 52072152, and 51802126), the Jiangsu University Jinshan Professor Fund, the Jiangsu Specially-Appointed Professor Fund, Open Fund from Guangxi Key Laboratory of Electrochemical Energy Materials, Zhenjiang "Jinshan Talents" Project 2021, China PostDoctoral Science Foundation (No. 2022M721372), "Doctor of Entrepreneurship and Innovation" in Jiangsu Province (No. JSSCBS20221197), and the Postgraduate Research & Practice Innovation Program of Jiangsu Province (Nos. KYCX22_3645 and KYCX24_3964).

Declaration of competing interest

All the contributing authors report no conflict of interests in this work.

Author contribution statement

X. W.: Data curation, validation, writing manuscript. Z. T.: Data curation, writing manuscript. Y. L.: Data curation, writing – review & editing. Y. Y.: Writing manuscript. Y. L.: Data curation. Y. C.: Writing manuscript. J. Y.: Writing – review & editing. N. L.: Funding acquisition, writing-review & editing. C. J.: Writing – review & editing. H. L.: Project administration, funding acquisition, writing – review & editing. All the authors have approved the final manuscript.

Informed consent

Not applicable.

Ethics statement

Not applicable.

Use of AI statement

None.

References

[1] Ren, X. Y.; Chen, D. X.; Wang, Y.; Li, H. F.; Zhang, Y. B.; Chen, H. Y.; Li, X.; Huo, M. F. Nanozymes-recent development and biomedical applications. *J. Nanobiotechnol.* **2022**, *20*, 92.

[2] Zhang, R. F.; Fan, K. L.; Yan, X. Y. Nanozymes: Created by learning from nature. *Sci. China Life Sci.* **2020**, *63*, 1183–1200.

[3] Zhao, K. Y.; Zhao, Y.; Wang, Y. W.; Han, B.; Lian, M. L. Progress in antibacterial applications of nanozymes. *Front. Chem.* **2024**, *12*, 1478273.

[4] Hamed, E. M.; Fung, F. M.; Li, S. F. Y. Unleashing the potential of single-atom nanozymes: Catalysts for the future. *ACS Sens.* **2024**, *9*, 3840–3847.

[5] Han, J. P.; Gu, Y. H.; Yang, C. Y.; Meng, L. C.; Ding, R. M.; Wang, Y. F.; Shi, K. R.; Yao, H. Q. Single-atom nanozymes: Classification, regulation strategy, and safety concerns. *J. Mater. Chem. B* **2023**, *11*, 9840–9866.

[6] Zeng, Q. D.; Zhong, H. H.; Liao, J. H.; Huo, Q.; Miao, B. P.; Zeng, L.; Zhang, B.; Nie, G. H. Antioxidant activities of metal single-atom nanozymes in biomedicine. *Biomater. Sci.* **2024**, *12*, 5150–5163.

[7] Jin, C. Y.; Fan, S. J.; Zhuang, Z. C.; Zhou, Y. S. Single-atom nanozymes: From bench to bedside. *Nano Res.* **2023**, *16*, 1992–2002.

[8] Li, H. T.; Kang, Z. H.; Liu, Y.; Lee, S. T. Carbon nanodots: Synthesis, properties and applications. *J. Mater. Chem.* **2012**, *22*, 24230–24253.

[9] Sun, X. C.; Lei, Y. Fluorescent carbon dots and their sensing applications. *TrAC Trends Anal. Chem.* **2017**, *89*, 163–180.

[10] Zhu, S. J.; Meng, Q. N.; Wang, L.; Zhang, J. H.; Song, Y. B.; Jin, H.; Zhang, K.; Sun, H. C.; Wang, H. Y.; Yang, B. Highly

photoluminescent carbon dots for multicolor patterning, sensors, and bioimaging. *Angew. Chem., Int. Ed.* **2013**, *52*, 3953–3957.

[11] Atchudan, R.; Edison, T. N. J. I.; Perumal, S.; Vinodh, R.; Sundramoorthy, A. K.; Babu, R. S.; Lee, Y. R. Leftover kiwi fruit peel-derived carbon dots as a highly selective fluorescent sensor for detection of ferric ion. *Chemosensors* **2021**, *9*, 166.

[12] Chen, H. X.; Zhu, X. L.; Zong, H. B.; Zeng, G. X.; Miao, H. H.; Mo, Z.; Hossain, M. S.; Yan, J.; Wang, L.; Xu, H. Strongly coupled NH_2NH-modified high crystallinity Graphene quantum dots/carbon nitride for efficient photocatalytic hydrogen evolution. *Int. J. Hydrogen Energy* **2023**, *48*, 36818–36824.

[13] Xiang, Y.; Cao, F.; Cao, J.; Chen, X. N.; XiOng, Q. Effects of high-temperature annealing on microstructure and mechanical property of SiO_2/SiO_2 composites. *Vacuum* **2017**, *144*, 1–7.

[14] Luo, L. J.; Liu, X. H.; Bi, X. Y.; Li, L. B.; You, T. Y. Facile fabrication and application of an innovative self-enhanced luminophore with outstanding electrochemiluminescence properties. *Sens. Actuators A: Phys.* **2020**, *312*, 112167.

[15] Gowthaman, N. S. K.; Sinduja, B.; Karthikeyan, R.; Rubini, K.; Abraham John, S. Fabrication of nitrogen-doped carbon dots for screening the purine metabolic disorder in human fluids. *Biosens. Bioelectron.* **2017**, *94*, 30–38.

[16] Zheng, M.; Ruan, S. B.; Liu, S.; Sun, T. T.; Qu, D.; Zhao, H. F.; Xie, Z. G.; Gao, H. L.; Jing, X. B.; Sun, Z. C. Self-targeting fluorescent carbon dots for diagnosis of brain cancer cells. *ACS Nano* **2015**, *9*, 11455–11461.

[17] Li, L. P.; Lu, C. X.; Li, S. J.; Liu, S. J.; Wang, L. J. E.; Cai, W. W.; Xu, W.; Yang, X.; Liu, Y. D.; Zhang, R. P. A high-yield and versatile method for the synthesis of carbon dots for bioimaging applications. *J. Mater. Chem. B* **2017**, *5*, 1935–1942.

[18] Baker, S. N.; Baker, G. A. Luminescent carbon nanodots: Emergent nanolights. *Angew. Chem., Int. Ed.* **2010**, *49*, 6726–6744.

[19] Hu, L. M.; Sun, Y.; Li, S. L.; Wang, X. L.; Hu, K. L.; Wang, L. R.; Liang, X. J.; Wu, Y. Multifunctional carbon dots with high quantum yield for imaging and gene delivery. *Carbon* **2014**, *67*, 508–513.

[20] Nguyen, H. V.; Richtera, L.; Moulick, A.; Xhaxhiu, K.; Kudr, J.; Cernei, N.; Polanska, H.; Heger, Z.; Masarik, M.; Kopel, P. et al. Electrochemical sensing of etoposide using carbon quantum dot modified glassy carbon electrode. *Analyst* **2016**, *141*, 2665–2675.

[21] Tetsuka, H.; Asahi, R.; Nagoya, A.; Okamoto, K.; Tajima, I.; Ohta, R.; Okamoto, A. Optically tunable amino-functionalized graphene quantum dots. *Adv. Mater.* **2012**, *24*, 5333–5338.

[22] Li, P. F.; Sun, L.; Xue, S. S.; Qu, D.; An, L.; Wang, X. Y.; Sun, Z. C. Recent advances of carbon dots as new antimicrobial agents. *SmartMat* **2022**, *3*, 226–248.

[23] Zhou, J.; Zhou, H.; Tang, J. B.; Deng, S. E.; Yan, F.; Li, W. J.; Qu, M. H. Carbon dots doped with heteroatoms for fluorescent bioimaging: A review. *Microchim. Acta* **2017**, *184*, 343–368.

[24] Zhang, Z. T.; Yi, G. Y.; Li, P.; Zhang, X. X.; Fan, H. Y.; Zhang, Y. L.; Wang, X. D.; Zhang, C. X. A minireview on doped carbon dots for photocatalytic and electrocatalytic applications. *Nanoscale* **2020**, *12*, 13899–13906.

[25] Mohammadinejad, R.; Dadashzadeh, A.; Moghassemi, S.; Ashrafizadeh, M.; Dehshahri, A.; Pardakhty, A.; Sassan, H.; Sohrevardi, S. M.; Mandegary, A. Shedding light on gene therapy: Carbon dots for the minimally invasive image-guided delivery of plasmids and noncoding RNAs - a review. *J. Adv. Res.* **2019**, *18*, 81–93.

[26] Que, X. Y.; Fu, F. M.; Yang, G. R.; Lei, B. F.; Ali, S.; Wang, X. M. A positively charged carbon dot complex improves the bioactivity of *Isaria fumosorosea* against *Plutella xylostella* (Linnaeus). *Chem. Biol. Technol. Agric.* **2024**, *11*, 192.

[27] Ma, J.; Kang, K.; Zhang, Y. J.; Yi, Q. Y.; Gu, Z. W. Detachable polyzwitterion-coated ternary nanoparticles based on peptide dendritic carbon dots for efficient drug delivery in cancer therapy. *ACS Appl. Mater. Interfaces* **2018**, *10*, 43923–43935.

[28] Chowdhury, D.; Gogoi, N.; Majumdar, G. Fluorescent carbon dots obtained from chitosan gel. *RSC Adv.* **2012**, *2*, 12156–12159.

[29] Sahiner, N.; Suner, S. S.; Sahiner, M.; Silan, C. Nitrogen and sulfur doped carbon dots from amino acids for potential biomedical applications. *J. Fluoresc.* **2019**, *29*, 1191–1200.

[30] Guo, R. B.; Chen, B.; Li, F. L.; Weng, S. H.; Zheng, Z. F.; Chen, M.; Wu, W.; Lin, X. H.; Yang, C. Y. Positive carbon dots with dual roles of nanoquencher and reference signal for the ratiometric fluorescence sensing of DNA. *Sens. Actuators B: Chem.* **2018**, *264*, 193–201.

[31] Jian, H. J.; Wu, R. S.; Lin, T. Y.; Li, Y. J.; Lin, H. J.; Harroun, S. G.; Lai, J. Y.; Huang, C. C. Super-cationic carbon quantum dots synthesized from spermidine as an eye drop formulation for topical treatment of bacterial keratitis. *ACS Nano* **2017**, *11*, 6703–6716.

[32] Chen, Y. C.; Chen, H. H.; Lin, H. J.; Huang, C. C.; Chen, K. F.; Peng, Y. P.; Tsang, Y. F.; Chen, Y. H.; Lin, K. Y. A.; Lin, C. H. Hepatotoxicity evaluations of different surface charged carbon quantum dots *in vivo* and *in vitro*. *Colloids Surf. B: Biointerfaces* **2024**, *234*, 113760.

[33] Jiang, P. L.; Hong, Y. Y.; Yang, L. Y.; Lin, H. J.; Huang, C. C.; Chen, Y. H.; Lin, C. H.; Chen, Y. C. Comprehensive evaluation of the nephrotoxicity of carbon quantum dots: Effects of the surface charge. *Chemosphere* **2024**, *367*, 143604.

[34] Li, X. C.; Fu, Y. Z.; Zhao, S. J.; Xiao, J. F.; Lan, M. H.; Wang, B. H.; Zhang, K.; Song, X. Z.; Zeng, L. T. Metal ions-doped carbon dots: Synthesis, properties, and applications. *Chem. Eng. J.* **2022**, *430*, 133101.

[35] Yu, J.; Huang, X.; Chen, X. H.; Hu, P. Y.; Liu, T.; Zhang, T. T.; Cheng, R.; Cui, T. T.; Li, J. Antibacterial and anti-inflammatory Bi-functional carbon dots hydrogel dressing for robust promotion of wound healing. *Carbon* **2024**, *226*, 119202.

[36] Shi, Y. P.; Pan, Y.; Zhong, J.; Yang, J.; Zheng, J. H.; Cheng, J. L.; Song, R.; Yi, C. Q. Facile synthesis of gadolinium (III) chelates functionalized carbon quantum dots for fluorescence and magnetic resonance dual-modal bioimaging. *Carbon* **2015**, *93*, 742–750.

[37] Sun, H. Z.; Wu, P. Y. Tuning the functional groups of carbon quantum dots in thin film nanocomposite membranes for nanofiltration. *J. Membr. Sci.* **2018**, *564*, 394–403.

[38] Zhu, S. J.; Song, Y. B.; Zhao, X. H.; Shao, J. R.; Zhang, J. H.; Yang, B. The photoluminescence mechanism in carbon dots (graphene quantum dots, carbon nanodots, and polymer dots): Current state and future perspective. *Nano Res.* **2015**, *8*, 355–381.

[39] Zhang, Y.; Zhao, J. R.; Sun, X. B.; Pan, W.; Yu, G. F.; Wang, J. P. Fluorescent carbon dots for probing the effect of thiram on the membrane of fungal cell and its quantitative detection in aqueous solution. *Sens. Actuators B: Chem.* **2018**, *273*, 1833–1842.

[40] Kudr, J.; Richtera, L.; Xhaxhiu, K.; Hynek, D.; Heger, Z.; Zitka, O.; Adam, V. Carbon dots based FRET for the detection of DNA damage. *Biosens. Bioelectron.* **2017**, *92*, 133–139.

[41] Bahadur, R.; Kumawat, M. K.; Thakur, M.; Srivastava, R. Multi-fluorescent cationic carbon dots for solid-state fingerprinting. *J. Lumin.* **2019**, *208*, 428–436.

[42] Zhai, X. Y.; Zhang, P.; Liu, C. J.; Bai, T.; Li, W. C.; Dai, L. M.; Liu, W. G. Highly luminescent carbon nanodots by microwave-assisted pyrolysis. *Chem. Commun.* **2012**, *48*, 7955–7957.

[43] Pierrat, P.; Wang, R. R.; Kereselidze, D.; Lux, M.; Didier, P.; Kichler, A.; Pons, F.; Lebeau, L. Efficient *in vitro* and *in vivo* pulmonary delivery of nucleic acid by carbon dot-based nanocarriers. *Biomaterials* **2015**, *51*, 290–302.

[44] Kasprzyk, W.; Bednarz, S.; Żmudzki, P.; Galica, M.; Bogdał, D. Novel efficient fluorophores synthesized from citric acid. *RSC Adv.* **2015**, *5*, 34795–34799.

[45] Qian, Z. S.; Ma, J. J.; Shan, X. Y.; Feng, H.; Shao, L. X.; Chen, J. R. Highly luminescent N-doped carbon quantum dots as an effective multifunctional fluorescence sensing platform. *Chem. -Eur. J.* **2014**, *20*, 2254–2263.

[46] Xue, W.; Lin, Z.; Chen, H.; Lu, C.; Lin, J. M. Enhancement of ultraweak chemiluminescence from reaction of hydrogen peroxide

and bisulfite by water-soluble carbon nanodots. *J. Phys. Chem. C* **2011**, *115*, 21707–21714.

[47] Ran, H. H.; Cheng, X. T.; Bao, Y. W.; Hua, X. W.; Gao, G.; Zhang, X. D.; Jiang, Y. W.; Zhu, Y. X.; Wu, F. G. Multifunctional quaternized carbon dots with enhanced biofilm penetration and eradication efficiencies. *J. Mater. Chem. B* **2019**, *7*, 5104–5114.

[48] Zhou, J.; Deng, W. W.; Wang, Y.; Cao, X.; Chen, J. J.; Wang, Q.; Xu, W. Q.; Du, P.; Yu, Q. T.; Chen, J. X. et al. Cationic carbon quantum dots derived from alginate for gene delivery: One-step synthesis and cellular uptake. *Acta Biomater.* **2016**, *42*, 209–219.

[49] Yang, X. D.; Wang, Y.; Shen, X. R.; Su, C. Y.; Yang, J. H.; Piao, M.; Jia, F.; Gao, G. H.; Zhang, L.; Lin, Q. One-step synthesis of photoluminescent carbon dots with excitation-independent emission for selective bioimaging and gene delivery. *J. Colloid Interface Sci.* **2017**, *492*, 1–7.

[50] Li, H.; Kong, W. Q.; Liu, J.; Liu, N. Y.; Huang, H.; Liu, Y.; Kang, Z. H. Fluorescent N-doped carbon dots for both cellular imaging and highly-sensitive catechol detection. *Carbon* **2015**, *91*, 66–75.

[51] Reddy, A. L. M.; Srivastava, A.; Gowda, S. R.; Gullapalli, H.; Dubey, M.; Ajayan, P. M. Synthesis of nitrogen-doped graphene films for lithium battery application. *ACS Nano* **2010**, *4*, 6337–6342.

[52] Li, Y.; Zhao, Y.; Cheng, H. H.; Hu, Y.; Shi, G. Q.; Dai, L. M.; Qu, L. T. Nitrogen-doped graphene quantum dots with oxygen-rich functional groups. *J. Am. Chem. Soc.* **2012**, *134*, 15–18.

[53] Robinson, J. T.; Burgess, J. S.; Junkermeier, C. E.; Badescu, S. C.; Reinecke, T. L.; Perkins, F. K.; Zalalutdniov, M. K.; Baldwin, J. W.; Culbertson, J. C.; Sheehan, P. E. et al. Properties of fluorinated graphene films. *Nano Lett.* **2010**, *10*, 3001–3005.

[54] Long, P.; Feng, Y. Y.; Cao, C.; Li, Y.; Han, J. K.; Li, S. W.; Peng, C.; Li, Z. Y.; Feng, W. Self-protective room-temperature phosphorescence of fluorine and nitrogen codoped carbon dots. *Adv. Funct. Mater.* **2018**, *28*, 1800791.

[55] O'Hagan, D. Understanding organofluorine chemistry. An introduction to the C–F bond. *Chem. Soc. Rev.* **2008**, *37*, 308–319.

[56] Li, H.; Wang, H. B.; Guo, J. Q.; Ye, S.; Shi, W. L.; Peng, X.; Song, J.; Qu, J. L. Long-wavelength excitation of carbon dots as the probe for real-time imaging of the living-cell cycle process. *Sens. Actuators B: Chem.* **2020**, *311*, 127891.

[57] Sun, B. H.; Wu, F.; Zhang, Q. C.; Chu, X. H.; Wang, Z. X.; Huang, X. R.; Li, J.; Yao, C.; Zhou, N. L.; Shen, J. Insight into the effect of particle size distribution differences on the antibacterial activity of carbon dots. *J. Colloid Interface Sci.* **2021**, *584*, 505–519.

[58] Geng, B. J.; Qin, H.; Shen, W. W.; Li, P.; Fang, F. L.; Li, X. K.; Pan, D. Y.; Shen, L. X. Carbon dot/WS_2 heterojunctions for NIR-II enhanced photothermal therapy of osteosarcoma and bone regeneration. *Chem. Eng. J.* **2020**, *383*, 123102.

[59] Yang, Q. Y.; Liu, J. W.; Cai, W. T.; Liang, X.; Zhuang, Z. C.; Liao, T.; Zhang, F. X.; Hu, W. K.; Liu, P. X.; Fan, S. J. et al. Non-heme iron single-atom nanozymes as peroxidase mimics for tumor catalytic therapy. *Nano Lett.* **2023**, *23*, 8585–8592.

[60] Zhuang, Z. C.; Wang, D. S. Advancing hydrogen energy through enzyme-mimetic electrocatalysis. *Front. Energy*, in press, DOI: 10.1007/s11708-025-0975-7.

[61] Chen, G.; Khan, I. M.; He, W. S.; Li, Y. X.; Jin, P.; Campanella, O. H.; Zhang, H. H.; Huo, Y. R.; Chen, Y.; Yang, H. Q. et al. Rebuilding the lid region from conformational and dynamic features to engineering applications of lipase in foods: Current status and future prospects. *Compr. Rev. Food Sci. Food Saf.* **2022**, *21*, 2688–2714.

[62] Han, J.; Feng, H.; Wu, J. C.; Li, Y. Y.; Zhou, Y.; Wang, L.; Luo, P.; Wang, Y. Construction of multienzyme co-immobilized hybrid nanoflowers for an efficient conversion of cellulose into glucose in a cascade reaction. *J. Agric. Food Chem.* **2021**, *69*, 7910–7921.

[63] Ngolong Ngea, G. L.; Yang, Q. Y.; Castoria, R.; Zhang, X. Y.; Routledge, M. N.; Zhang, H. Y. Recent trends in detecting, controlling, and detoxifying of patulin mycotoxin using biotechnology methods. *Compr. Rev. Food Sci. Food Saf.* **2020**, *19*, 2447–2472.

[64] Ouyang, Q.; Wang, L.; Ahmad, W.; Rong, Y. W.; Li, H. H.; Hu, Y. Q.; Chen, Q. S. A highly sensitive detection of carbendazim pesticide in food based on the upconversion-MnO_2 luminescent resonance energy transfer biosensor. *Food Chem.* **2021**, *349*, 129157.

[65] Xu, Y.; Hassan, M. M.; Sharma, A. S.; Li, H. H.; Chen, Q. S. Recent advancement in nano-optical strategies for detection of pathogenic bacteria and their metabolites in food safety. *Compr. Rev. Food Sci. Nutr.* **2023**, *63*, 486–504.

[66] Zhu, W. R.; Li, L. B.; Zhou, Z.; Yang, X. D.; Hao, N.; Guo, Y. S.; Wang, K. A colorimetric biosensor for simultaneous ochratoxin A and aflatoxins B1 detection in agricultural products. *Food Chem.* **2020**, *319*, 126544.

[67] Hu, X. T.; Li, Y. X.; Xu, Y. W.; Gan, Z. Y.; Zou, X. B.; Shi, J. Y.; Huang, X. W.; Li, Z. H.; Li, Y. H. Green one-step synthesis of carbon quantum dots from orange peel for fluorescent detection of *Escherichia coli* in milk. *Food Chem.* **2021**, *339*, 127775.

[68] Hu, X. T.; Shi, J. Y.; Shi, Y. Q.; Zou, X. B.; Arslan, M.; Zhang, W.; Huang, X. W.; Li, Z. H.; Xu, Y. W. Use of a smartphone for visual detection of melamine in milk based on Au@Carbon quantum dots nanocomposites. *Food Chem.* **2019**, *272*, 58–65.

[69] Li, X. C.; Zhao, S. J.; Li, B. L.; Yang, K.; Lan, M. H.; Zeng, L. T. Advances and perspectives in carbon dot-based fluorescent probes: Mechanism, and application. *Coord. Chem. Rev.* **2021**, *431*, 213686.

[70] Jiang, T. Y.; Li, L. X.; Li, L. H.; Liu, Y. H.; Zhang, D. X.; Zhang, D. Q.; Li, H. T.; Mao, B. D.; Shi, W. D. Ultra-thin shelled $Cu_{2-x}S/MoS_2$ quantum dots for enhanced electrocatalytic nitrogen reduction. *Chem. Eng. J.* **2021**, *426*, 130650.

[71] Li, L. B.; Zhao, W. L.; Wang, Y.; Liu, X. H.; Jiang, P. N.; Luo, L. J.; Bi, X. Y.; Meng, X. L.; Niu, Q. J.; Wu, X. F. et al. Gold nanocluster-confined covalent organic frameworks as bifunctional probes for electrochemiluminescence and colorimetric dual-response sensing of Pb^{2+}. *J. Hazard. Mater.* **2023**, *457*, 131558.

[72] Cao, H. W.; Wang, X. X.; Liu, J.; Sun, Z.; Yu, Z. Q.; Battino, M.; El‐Seedi, H.; Guan, X. Mechanistic insights into the changes of enzyme activity in food processing under microwave irradiation. *Compr. Rev. Food Sci. Food Saf.* **2023**, *22*, 2465–2487.

[73] Liang, N. N.; Hu, X. T.; Li, W. T.; Mwakosya, A. W.; Guo, Z. A.; Xu, Y. W.; Huang, X. W.; Li, Z. H.; Zhang, X. N.; Zou, X. B. et al. Fluorescence and colorimetric dual-mode sensor for visual detection of malathion in cabbage based on carbon quantum dots and gold nanoparticles. *Food Chem.* **2021**, *343*, 128494.

[74] Sharma, A. S.; Ali, S.; Sabarinathan, D.; Murugavelu, M.; Li, H. H.; Chen, Q. S. Recent progress on graphene quantum dots‐based fluorescence sensors for food safety and quality assessment applications. *Compr. Rev. Food Sci. Food Saf.* **2021**, *20*, 5765–5801.

[75] Wang, S. L.; Liang, N. N.; Hu, X. T.; Li, W. T.; Guo, Z. A.; Zhang, X. N.; Huang, X. W.; Li, Z. H.; Zou, X. B.; Shi, J. Y. Carbon dots and covalent organic frameworks based FRET immunosensor for sensitive detection of *Escherichia coli* O157:H7. *Food Chem.* **2024**, *447*, 138663.

[76] Lu, W. J.; Guo, Y. J.; Zhang, J. H.; Yue, Y. F.; Fan, L.; Li, F.; Dong, C.; Shuang, S. M. A high catalytic activity nanozyme based on cobalt-doped carbon dots for biosensor and anticancer cell effect. *ACS Appl. Mater. Interfaces* **2022**, *14*, 57206–57214.

[77] Yang, W. Q.; Ni, J. C.; Luo, F.; Weng, W.; Wei, Q. H.; Lin, Z. Y.; Chen, G. N. Cationic carbon dots for modification-free detection of hyaluronidase via an electrostatic-controlled ratiometric fluorescence assay. *Anal. Chem.* **2017**, *89*, 8384–8390.

[78] Raj, P.; Lee, S. Y.; Lee, T. Y. Carbon dot/naphthalimide based ratiometric fluorescence biosensor for hyaluronidase detection. *Materials* **2021**, *14*, 1313.

[79] Siotto, M.; Squitti, R. Copper imbalance in Alzheimer's disease: Overview of the exchangeable copper component in plasma and the intriguing role albumin plays. *Coord. Chem. Rev.* **2018**, *371*, 86–95.

[80] Squitti, R.; Ghidoni, R.; Simonelli, I.; Ivanova, I. D.; Colabufo, N. A.; Zuin, M.; Benussi, L.; Binetti, G.; Cassetta, E.; Rongioletti, M. et al. Copper dyshomeostasis in Wilson disease and Alzheimer's

disease as shown by serum and urine copper indicators. *J. Trace Elem. Med. Biol.* **2018**, *45*, 181–188.
[81] Ahuja, A.; Dev, K.; Tanwar, R. S.; Selwal, K. K.; Tyagi, P. K. Copper mediated neurological disorder: Visions into amyotrophic lateral sclerosis, Alzheimer and Menkes disease. *J. Trace Elem. Med. Biol.* **2015**, *29*, 11–23.
[82] Ilyechova, E. Y.; Miliukhina, I. V.; Orlov, I. A.; Muruzheva, Z. M.; Puchkova, L. V.; Karpenko, M. N. A low blood copper concentration is a co-morbidity burden factor in Parkinson's disease development. *Neurosci. Res.* **2018**, *135*, 54–62.
[83] Kim, M. J.; Oh, S. B.; Kim, J.; Kim, K.; Ryu, H. S.; Kim, M. S.; Ayton, S.; Bush, A. I.; Lee, J. Y.; Chung, S. J. Association of metals with the risk and clinical characteristics of Parkinson's disease. *Parkinsonism Relat. Disord.* **2018**, *55*, 117–121.
[84] Meng, H.; Wang, Y.; Wu, R. X.; Li, Y. M.; Wei, D. L.; Li, M. W.; Zhu, N. F.; Zhu, F.; Zhang, Z.; Zhao, H. J. Identification of multi-component metal ion mixtures in complex systems using fluorescence sensor arrays. *J. Hazard. Mater.* **2023**, *455*, 131546.
[85] Feng, F.; Miao, C. F.; Zhang, Y. L.; Huang, Z. J.; Weng, S. H. Positively charged and pH-sensitive carbon dots for fluorescence detection of copper ion. *Bull. Korean Chem. Soc.* **2021**, *42*, 227–234.
[86] Parks, H. C. W.; McCoy, T. M.; Tabor, R. F. Carbon quantum dot assisted adsorption of graphene oxide to the oil-water interface for copper sensing emulsions. *Adv. Mater. Interfaces* **2019**, *6*, 1900392.
[87] Wang, L.; Cao, H. X.; He, Y. S.; Pan, C. G.; Sun, T. K.; Zhang, X. Y.; Wang, C. Y.; Liang, G. X. Facile preparation of amino-carbon dots/gold nanoclusters FRET ratiometric fluorescent probe for sensing of Pb^{2+}/Cu^{2+}. *Sens. Actuators B: Chem.* **2019**, *282*, 78–84.
[88] Han, B. Y.; Li, Y.; Hu, X. X.; Yan, Q.; Jiang, J. M.; Yu, M. B.; Peng, T. T.; He, G. H. Paper-based visual detection of silver ions and L-cysteine with a dual-emissive nanosystem of carbon quantum dots and gold nanoclusters. *Anal. Methods* **2018**, *10*, 3945–3950.
[89] Wu, X. L.; Song, Y.; Yan, X.; Zhu, C. Z.; Ma, Y. Q.; Du, D.; Lin, Y. H. Carbon quantum dots as fluorescence resonance energy transfer sensors for organophosphate pesticides determination. *Biosens. Bioelectron.* **2017**, *94*, 292–297.
[90] Dong, W. J.; Wang, R. P.; Gong, X. J.; Liang, W. T.; Dong, C. A far-red FRET fluorescent probe for ratiometric detection of L-cysteine based on carbon dots and *N*-acetyl-L-cysteine-capped gold nanoparticles. *Spectrochim. Acta A: Mol. Biomol. Spectrosc.* **2019**, *213*, 90–96.
[91] Li, Y. H.; Cai, J. B.; Liu, F. J.; Yang, H.; Lin, Y.; Li, S. X.; Huang, X. G.; Lin, L. X. Construction of a turn off-on fluorescent nanosensor for cholesterol based on fluorescence resonance energy transfer and competitive host-guest recognition. *Talanta* **2019**, *201*, 82–89.
[92] Wang, B.; Chen, Y. F.; Wu, Y. Y.; Weng, B.; Liu, Y. S.; Lu, Z. S.; Li, C. M.; Yu, C. Aptamer induced assembly of fluorescent nitrogen-doped carbon dots on gold nanoparticles for sensitive detection of AFB_1. *Biosens. Bioelectron.* **2016**, *78*, 23–30.
[93] Liu, S. S.; Li, H. H.; Hassan, M. M.; Ali, S.; Chen, Q. A. SERS based artificial peroxidase enzyme regulated multiple signal amplified system for quantitative detection of foodborne pathogens. *Food Control* **2021**, *123*, 107733.
[94] Yu, S.; Guo, F.; Luo, Y. Z.; Zhang, X. F.; Wang, C. Y.; Liu, Y. H.; Zhang, H. Y. Electropositive citric acid-polyethyleneimine carbon dots carrying the PINK1 gene regulate ATP-related metabolic dysfunction in APP/PS1-N2a cells. *Molecules* **2024**, *29*, 1907.
[95] Shen, J.; Zhang, G. M.; Zhang, Z. D.; Zhang, L. D.; Zhuang, Z. C.; Qian, Y. P.; Dou, Y. H.; Wang, S. B.; Wang, D. S.; Wang, Y. G. High-throughput screening and general synthesis strategy of single-atom nanozymes for oral squamous cell carcinoma therapy. *Adv. Mater.* **2025**, *37*, 2416463.
[96] Xia, J. K.; Xu, J. W.; Yu, B.; Liang, X.; Qiu, Z.; Li, H.; Feng, H. J.; Li, Y. F.; Cai, Y. J.; Wei, H. Y. et al. A metal-sulfur-carbon catalyst mimicking the two-component architecture of nitrogenase. *Angew. Chem., Int. Ed.* **2024**, *63*, e202412740.
[97] Iqbal, M. W.; Riaz, T.; Mahmood, S.; Bilal, M.; Manzoor, M. F.; Qamar, S. A.; Qi, X. H. Fucoidan-based nanomaterial and its multifunctional role for pharmaceutical and biomedical applications. *Compr. Rev. Food Sci. Nutr.* **2024**, *64*, 354–380.
[98] Marimuthu, M.; Arumugam, S. S.; Sabarinathan, D.; Li, H. H.; Chen, Q. S. Metal organic framework based fluorescence sensor for detection of antibiotics. *Trends Food Sci. Technol.* **2021**, *116*, 1002–1028.
[99] Wang, L.; Li, W. X.; Liu, Y. Y.; Zhi, W. J.; Han, J.; Wang, Y.; Ni, L. Green separation of bromelain in food sample with high retention of enzyme activity using recyclable aqueous two-phase system containing a new synthesized thermo-responsive copolymer and salt. *Food Chem.* **2019**, *282*, 48–57.
[100] Jing, Y. L.; Zhang, Y. H.; Han, I.; Wang, P.; Mei, Q. W.; Huang, Y. J. Effects of different straw biochars on soil organic carbon, nitrogen, available phosphorus, and enzyme activity in paddy soil. *Sci. Rep.* **2020**, *10*, 8837.
[101] Li, W. T.; Hu, X. T.; Li, Q.; Shi, Y. Q.; Zhai, X. D.; Xu, Y. W.; Li, Z. H.; Huang, X. W.; Wang, X.; Shi, J. Y. et al. Copper nanoclusters @ nitrogen-doped carbon quantum dots-based ratiometric fluorescence probe for lead (II) ions detection in porphyra. *Food Chem.* **2020**, *320*, 126623.
[102] Bourlinos, A. B.; Bakandritsos, A.; Kouloumpis, A.; Gournis, D.; Krysmann, M.; Giannelis, E. P.; Polakova, K.; Safarova, K.; Hola, K.; Zboril, R. Gd(III)-doped carbon dots as a dual fluorescent-MRI probe. *J. Mater. Chem.* **2012**, *22*, 23327–23330.
[103] Ren, X. Y.; Liu, L. H.; Li, Y.; Dai, Q.; Zhang, M.; Jing, X. L. Facile preparation of gadolinium(III) chelates functionalized carbon quantum dot-based contrast agent for magnetic resonance/fluorescence multimodal imaging. *J. Mater. Chem. B* **2014**, *2*, 5541–5549.
[104] Xu, Y.; Jia, X. H.; Yin, X. B.; He, X. W.; Zhang, Y. K. Carbon quantum dot stabilized gadolinium nanoprobe prepared via a one-pot hydrothermal approach for magnetic resonance and fluorescence dual-modality bioimaging. *Anal. Chem.* **2014**, *86*, 12122–12129.
[105] Gong, N. Q.; Wang, H.; Li, S.; Deng, Y. L.; Chen, X.; Ye, L.; Gu, W. Microwave-assisted polyol synthesis of gadolinium-doped green luminescent carbon dots as a bimodal nanoprobe. *Langmuir* **2014**, *30*, 10933–10939.
[106] Hanahan, D.; Weinberg, R. A. Hallmarks of cancer: The next generation. *Cell* **2011**, *144*, 646–674.
[107] Wang, L. M.; Wang, B. Z.; Liu, E. S.; Zhao, Y. Y.; He, B. C.; Wang, C. F.; Xing, G. C.; Tang, Z. K.; Zhou, Y. N.; Qu, S. N. Polyetherimide functionalized carbon dots with enhanced red emission in aqueous solution for bioimaging. *Chin. Chem. Lett.* **2022**, *33*, 4111–4115.
[108] Sun, J. B.; Li, H. C.; Ouyang, M.; Cheng, J.; Xu, D.; Tan, X. F.; Lin, Q. L. User-friendly multifunctional red-emissive carbon dots for rapid cell nucleus staining via targeting nuclear proteins. *Anal. Chem.* **2024**, *96*, 8432–8440.
[109] Zhu, Z. M.; Lin, X. Y.; Wu, L. N.; Zhao, C. F.; Li, S. G.; Liu, A. L.; Lin, X. H.; Lin, L. Q. Nitrogen-doped carbon dots as a ratiometric fluorescent probe for determination of the activity of acid phosphatase, for inhibitor screening, and for intracellular imaging. *Mikrochim. Acta* **2019**, *186*, 558.
[110] Hoan, B. T.; Tam, P. D.; Pham, V. H. Green synthesis of highly luminescent carbon quantum dots from lemon juice. *J. Nanotechnol.* **2019**, *2019*, 2852816.
[111] Fang, H. Y.; Huang, W. M.; Chen, D. H. One-step synthesis of positively charged bifunctional carbon dot/silver composite nanoparticles for killing and fluorescence imaging of gram-negative bacteria. *Nanotechnology* **2019**, *30*, 365603.
[112] Chen, Q.; Duan, X. M.; Yu, Y.; Ni, R. R.; Song, G. J.; Yang, X.; Zhu, L.; Zhong, Y.; Zhang, K.; Qu, K. et al. Target functionalized carbon dot nanozymes with dual-model photoacoustic and fluorescence imaging for visual therapy in atherosclerosis. *Adv. Sci.* **2024**, *11*, 2307441.

[113] Zhang, M. X.; Liang, Y. L.; Zhang, Y. N.; Zhang, L. M.; Wang, N.; Zhou, Y.; Wang, Y. F.; Cui, M. L.; Yu, Z. X.; Zhang, M. Z. et al. Oral carbon dot nanozymes with red fluorescence and superoxide dismutase-like activity for colitis bioimaging and inflammation management. *Chem. Eng. J.* **2024**, *493*, 152842.

[114] Li, Y.; Ma, W. S.; Sun, J.; Lin, M.; Niu, Y. S.; Yang, X. C.; Xu, Y. H. Electrochemical generation of Fe_3C/N-doped graphitic carbon nanozyme for efficient wound healing *in vivo*. *Carbon* **2020**, *159*, 149–160.

[115] Lu, J.; Qin, Y. Y.; Zhang, Q.; Yu, C.; Wu, Y. L.; Yan, Y. S.; Fan, H. G.; Meng, M. J.; Li, C. X. Antibacterial, high-flux and 3D porous molecularly imprinted nanocomposite sponge membranes for cross-flow filtration of emodin from analogues. *Chem. Eng. J.* **2019**, *360*, 483–493.

[116] Meziani, M. J.; Dong, X. L.; Zhu, L.; Jones, L. P.; LeCroy, G. E.; Yang, F.; Wang, S. Y.; Wang, P.; Zhao, Y. P.; Yang, L. J. et al. Visible-light-activated bactericidal functions of carbon "quantum" dots. *ACS Appl. Mater. Interfaces* **2016**, *8*, 10761–10766.

[117] Jijie, R.; Barras, A.; Bouckaert, J.; Dumitrascu, N.; Szunerits, S.; Boukherroub, R. Enhanced antibacterial activity of carbon dots functionalized with ampicillin combined with visible light triggered photodynamic effects. *Colloids Surf. B: Biointerfaces* **2018**, *170*, 347–354.

[118] Stanković, N. K.; Bodík, M.; Šiffalovič, P.; Kotlár, M.; Mičušík, M.; Špitálský, Z.; Danko, M.; Milivojević, D. D.; Kleinová, A.; Kubát, P. et al. Antibacterial and antibiofouling properties of light triggered fluorescent hydrophobic carbon quantum dots Langmuir-Blodgett thin films. *ACS Sustain. Chem. Eng.* **2018**, *6*, 4154–4163.

[119] Wang, C. B.; Li, Y. P.; Huang, L. Y.; Yang, L.; Wang, H.; Liu, J.; Liu, J. W.; Song, Z. W.; Huang, L. J. Enhanced photocatalytic antibacterial and degradation performance by n-p type 0D/2D SnO_{2-x}/BiOI photocatalyst under LED light. *Chem. Eng. J.* **2021**, *411*, 128505.

[120] Travlou, N. A.; Giannakoudakis, D. A.; Algarra, M.; Labella, A. M.; Rodríguez-Castellón, E.; Bandosz, T. J. S- and N-doped carbon quantum dots: Surface chemistry dependent antibacterial activity. *Carbon* **2018**, *135*, 104–111.

[121] Zhao, C. F.; Wang, X. W.; Wu, L. N.; Wu, W.; Zheng, Y. J.; Lin, L. Q.; Weng, S. H.; Lin, X. H. Nitrogen-doped carbon quantum dots as an antimicrobial agent against Staphylococcus for the treatment of infected wounds. *Colloids Surf. B: Biointerfaces* **2019**, *179*, 17–27.

[122] Hao, X. L.; Huang, L. L.; Zhao, C. F.; Chen, S. N.; Lin, W. J.; Lin, Y. N.; Zhang, L. R.; Sun, A.; Miao, C. F.; Lin, X. H. et al. Antibacterial activity of positively charged carbon quantum dots without detectable resistance for wound healing with mixed bacteria infection. *Mater. Sci. Eng.: C* **2021**, *123*, 111971.

[123] Feng, T.; Ai, X. Z.; An, G. H.; Yang, P. P.; Zhao, Y. L. Charge-convertible carbon dots for imaging-guided drug delivery with enhanced *in vivo* cancer therapeutic efficiency. *ACS Nano* **2016**, *10*, 4410–4420.

[124] Barras, A.; Sauvage, F.; de Hoon, I.; Braeckmans, K.; Hua, D. W.; Buvat, G.; Fraire, J. C.; Lethien, C.; Sebag, J.; Harrington, M. et al. Carbon quantum dots as a dual platform for the inhibition and light-based destruction of collagen fibers: Implications for the treatment of eye floaters. *Nanoscale Horiz.* **2021**, *6*, 449–461.

[125] Lei, H.; Alu, A.; Yang, J. Y.; He, X.; He, C.; Ren, W. Y.; Chen, Z. M.; Hong, W. Q.; Chen, L.; He, X. M. et al. Cationic crosslinked carbon dots-adjuvanted intranasal vaccine induces protective immunity against Omicron-included SARS-CoV-2 variants. *Nat. Commun.* **2023**, *14*, 2678.

[126] Guerra, J.; Herrero, M. A.; Vázquez, E. Carbon nanohorns as alternative gene delivery vectors. *RSC Adv.* **2014**, *4*, 27315–27321.

[127] Mehta, V. N.; Jha, S.; Kailasa, S. K. One-pot green synthesis of carbon dots by using *Saccharum officinarum* juice for fluorescent imaging of bacteria (*Escherichia coli*) and yeast (*Saccharomyces cerevisiae*) cells. *Mater. Sci. Eng.: C* **2014**, *38*, 20–27.

[128] Mehta, V. N.; Jha, S.; Singhal, R. K.; Kailasa, S. K. Preparation of multicolor emitting carbon dots for HeLa cell imaging. *New J. Chem.* **2014**, *38*, 6152–6160.

[129] Mehta, V. N.; Jha, S.; Basu, H.; Singhal, R. K.; Kailasa, S. K. One-step hydrothermal approach to fabricate carbon dots from apple juice for imaging of mycobacterium and fungal cells. *Sens. Actuators B: Chem.* **2015**, *213*, 434–443.

[130] Peng, J. X.; Wang, H. H.; Cao, H. X.; Liu, P. F.; Wang, H. Y.; Zhao, K. R.; Wang, L. A tandem DNA nanomachines-supported electrochemiluminescence assay for attomolar detection of miRNA at ambient-temperature. *Chem. Eng. J.* **2024**, *480*, 148161.

[131] Tao, Y.; Li, Z. H.; Ju, E. G.; Ren, J. S.; Qu, X. G. Polycations-functionalized water-soluble gold nanoclusters: A potential platform for simultaneous enhanced gene delivery and cell imaging. *Nanoscale* **2013**, *5*, 6154–6160.

[132] Miao, L.; Zhang, K.; Qiao, C.; Jin, X.; Zheng, C.; Yang, B.; Sun, H. Antitumor effect of human TRAIL on adenoid cystic carcinoma using magnetic nanoparticle-mediated gene expression. *Nanomed.: Nanotechnol. Biol. Med.* **2013**, *9*, 141–150.

[133] Posadas, I.; Guerra, F. J.; Ceña, V. Nonviral vectors for the delivery of small interfering RNAs to the CNS. *Nanomedicine* **2010**, *5*, 1219–1236.

[134] Liang, Q. H.; Ma, W. J.; Shi, Y.; Li, Z.; Yang, X. M. Easy synthesis of highly fluorescent carbon quantum dots from gelatin and their luminescent properties and applications. *Carbon* **2013**, *60*, 421–428.

[135] Diroll, B. T.; Murray, C. B. High-temperature photoluminescence of CdSe/CdS core/shell nanoheterostructures. *ACS Nano* **2014**, *8*, 6466–6474.

[136] Naraginti, S.; Yu, Y. Y.; Fang, Z.; Yong, Y. C. Novel tetrahedral Ag_3PO_4@N-rGO for photocatalytic detoxification of sulfamethoxazole: Process optimization, transformation pathways and biotoxicity assessment. *Chem. Eng. J.* **2019**, *375*, 122035.

[137] Cao, X.; Deng, W. W.; Qu, R.; Yu, Q. T.; Li, J.; Yang, Y.; Cao, Y.; Gao, X. D.; Xu, X. M.; Yu, J. N. Non-viral co-delivery of the four yamanaka factors for generation of human induced pluripotent stem cells via calcium phosphate nanocomposite particles. *Adv. Funct. Mater.* **2013**, *23*, 5403–5411.

[138] Deng, W. W.; Fu, M.; Cao, Y.; Cao, X.; Wang, M.; Yang, Y.; Qu, R.; Li, J.; Xu, X. M.; Yu, J. N. *Angelica sinensis* polysaccharide nanoparticles as novel non-viral carriers for gene delivery to mesenchymal stem cells. *Nanomed.: Nanotechnol. Biol. Med.* **2013**, *9*, 1181–1191.

[139] Shu, M. J.; Gao, F.; Yu, C. L.; Zeng, M.; He, G. L.; Wu, Y.; Su, Y. J.; Hu, N. T.; Zhou, Z. H.; Yang, Z. et al. Dual-targeted therapy in HER2-positive breast cancer cells with the combination of carbon dots/HER3 siRNA and trastuzumab. *Nanotechnology* **2020**, *31*, 335102.

[140] Algarra, M.; Gonzalez-Muñoz, E. Efficient and scalable gene delivery method with easily generated cationic carbon dots. *Biol. Proced. Online* **2024**, *26*, 6.

[141] Wang, J.; Liu, S. Y.; Chang, Y.; Fang, L.; Han, K.; Li, M. High efficient delivery of siRNA into tumor cells by positively charged carbon dots. *J. Macromol. Sci. A* **2018**, *55*, 770–774.

[142] Chen, J. Y.; Li, F.; Zhao, B. W.; Gu, J.; Brejcha, N. M.; Bartoli, M.; Zhang, W.; Zhou, Y. Q.; Fu, S. W.; Domena, J. B. et al. Gene transfection efficiency improvement with lipid conjugated cationic carbon dots. *ACS Appl. Mater. Interfaces* **2024**, *16*, 27087–27101.

[143] Goy-López, S.; Juárez, J.; Alatorre-Meda, M.; Casals, E.; Puntes, V. F.; Taboada, P.; Mosquera, V. Physicochemical characteristics of protein-NP bioconjugates: The role of particle curvature and solution conditions on human serum albumin conformation and fibrillogenesis inhibition. *Langmuir* **2012**, *28*, 9113–9126.

[144] Sun, H. H.; Zhang, J.; Zhang, Y. Z.; Yang, L. Y.; Yuan, L. L.; Liu, Y. Interaction of human serum albumin with 10-hydroxycamptothecin: Spectroscopic and molecular modeling studies. *Mol. Biol. Rep.* **2012**, *39*, 5115–5123.

[145] Li, M. Y.; Xiao, C. Q.; Xu, Z. Q.; Yin, M. M.; Yang, Q. Q.; Yin, Y. L.; Liu, Y. Role of surface charge on the interaction between carbon

nanodots and human serum albumin. *Spectrochim. Acta A: Mol. Biomol. Spectrosc.* **2018**, *204*, 484–494.

[146] Liu, N. Y.; Wu, R. Q.; Liu, Y. X.; Liu, Y. L.; Deng, P. J.; Li, Y. X.; Du, Y. C.; Cheng, Y. Y.; Zhuang, Z. C.; Kang, Z. H. et al. Oxygen vacancy engineering of Fe-doped $NiMoO_4$ for electrocatalytic N_2 fixation to NH_3. *Inorg. Chem.* **2023**, *62*, 11990–12000.

[147] Liu, Y. L.; Zhuang, Z. C.; Liu, Y. X.; Liu, N. Y.; Li, Y. X.; Cheng, Y. Y.; Yu, J. W.; Yu, R. H.; Wang, D. S.; Li, H. T. Shear-strained Pd single-atom electrocatalysts for nitrate reduction to ammonia. *Angew. Chem., Int. Ed.* **2024**, *63*, e202411396.

[148] Lang, Z. Q.; Wang, X. X.; Jabeen, S.; Cheng, Y. Y.; Liu, N. Y.; Liu, Z. H.; Gan, T.; Zhuang, Z. C.; Li, H. T.; Wang, D. S. Destabilization of single-atom catalysts: Characterization, mechanisms, and regeneration strategies. *Adv. Mater.*, in press, DOI: 10.1002/adma.202418942.

[149] Li, Y. X.; Liu, Y. X.; Liu, X.; Liu, Y. L.; Cheng, Y. Y.; Zhang, P.; Deng, P. J.; Deng, J. J.; Kang, Z. H.; Li, H. T. Fe-doped SnO_2 nanosheet for ambient electrocatalytic nitrogen reduction reaction. *Nano Res.* **2022**, *15*, 6026–6035.

[150] Tang, G.; Wang, J. L.; Xiao, J. H.; Liu, Y. L.; Huang, Y. Q.; Zhou, Z. Y.; Zhang, X. H.; Hu, G. H.; Yan, W. Y.; Cao, Y. S. Amphiphilic cationic carbon dots for efficient delivery of light-dependent herbicide. *Adv. Sci.* **2024**, *11*, 2406523.

[151] Xiao, X. F.; Zhuang, Z. C.; Yin, S. H.; Zhu, J. X.; Gan, T.; Yu, R. H.; Wu, J. S.; Tian, X. C.; Jiang, Y. X.; Wang, D. S. et al. Topological transformation of microbial proteins into iron single-atom sites for selective hydrogen peroxide electrosynthesis. *Nat. Commun.* **2024**, *15*, 10758.

[152] Otero, P.; Carpena, M.; Garcia-Oliveira, P.; Echave, J.; Soria-Lopez, A.; Garcia-Perez, P.; Fraga-Corral, M.; Cao, H.; Nie, S. P.; Xiao, J. B. et al. Seaweed polysaccharides: Emerging extraction technologies, chemical modifications and bioactive properties. *Compr. Rev. Food Sci. Nutr.* **2023**, *63*, 1901–1929.

[153] Wu, Y. Q.; Zhang, J. J.; Hu, X. T.; Huang, X. W.; Zhang, X. N.; Zou, X. B.; Shi, J. Y. Preparation of edible antibacterial films based on corn starch/carbon nanodots for bioactive food packaging. *Food Chem.* **2024**, *444*, 138467.

[154] Liu, Y. L.; Zheng, Z. Y.; Jabeen, S.; Liu, N. Y.; Liu, Y. X.; Cheng, Y. Y.; Li, Y. X.; Yu, J. W.; Wu, X.; Yan, N. N. et al. Mechanochemical route to fabricate an efficient nitrate reduction electrocatalyst. *Nano Res.* **2024**, *17*, 4889–4897.

[155] Hao, J. C.; Wang, T. D.; Cai, J.; Gao, G. H.; Zhuang, Z. C.; Yu, R. H.; Wu, J. S.; Wu, G. M.; Lu, S. L.; Wang, X. F. et al. Suppression of structural heterogeneity in high-entropy intermetallics for electrocatalytic upgrading of waste plastics. *Angew. Chem., Int. Ed.* **2025**, *64*, e202419369.

[156] Hao, J. C.; Wang, T. D.; Yu, R. H.; Cai, J.; Gao, G. H.; Zhuang, Z. C.; Kang, Q.; Lu, S. L.; Liu, Z. H.; Wu, J. S. et al. Integrating few-atom layer metal on high-entropy alloys to catalyze nitrate reduction in tandem. *Nat. Commun.* **2024**, *15*, 9020.

[157] Cheng, Y. Y.; Jabeen, S.; Lei, S. W.; Liu, N. Y.; Liu, Y. X.; Liu, Y. L.; Li, Y. X.; Wu, X.; Tong, Z.; Yu, J. W. et al. N-doped carbon dots-modulated interfacial charge transfer and surface structure in $FeNbO_4$ photocatalysts for enhanced CO_2 conversion selectivity to CH_4. *Chem. Eng. J.* **2024**, *498*, 155576.

[158] Tong, Z.; Liu, Y. L.; Wu, X.; Cheng, Y. Y.; Yu, J. W.; Zhang, X. Y.; Liu, N. Y.; Liu, X.; Li, H. T. Carbon quantum dots/Cu_2O photocatalyst for room temperature selective oxidation of benzyl alcohol. *Nanomaterials* **2024**, *14*, 212.

[159] Madonia, A.; Martin-Sabi, M.; Sadaoui, A.; Ruhlmann, L.; Ammar, S.; Schaming, D. Dawson-type polyoxometalates photosensitized with carbon dots for photocatalytic reduction of silver ions. *Mater. Res. Bull.* **2022**, *149*, 111721.

[160] Zhao, S. D.; Chen, J. R.; Liu, Y. F.; Jiang, Y.; Jiang, C. G.; Yin, Z. L.; Xiao, Y. G.; Cao, S. S. Silver nanoparticles confined in shell-in-shell hollow TiO_2 manifesting efficiently photocatalytic activity and stability. *Chem. Eng. J.* **2019**, *367*, 249–259.

[161] Hu, W.; Che, G. B.; Che, H. N.; Hu, H.; Jiang, E. H.; Ruan, X. W.; Zhang, X. X.; Liu, C. B.; Dong, H. J. Construction of mesoporous NCQDs-BiOCL composites for photocatalytic-degrading organic pollutants in water under visible and near-infrared light. *J. Environ. Eng.* **2019**, *145*, 04019031.

[162] Gocyla, M.; Dolinska, J.; Rostkowska, N.; Opallo, M. Electrochemical detection of positively charged carbon nanoparticles suspension in flow. *Electroanalysis* **2018**, *30*, 1965–1970.

[163] Gan, H.; Han, W. Z.; Fu, Z. D.; Wang, L. P. The chain-like Au/carbon dots nanocomposites with peroxidase-like activity and their application for glucose detection. *Colloids Surf. B: Biointerfaces* **2021**, *199*, 111553.

[164] Wang, Y. T.; Li, T. L.; Lin, L. X.; Wang, D.; Feng, L. Y. Copper-doped cherry blossom carbon dots with peroxidase-like activity for antibacterial applications. *RSC Adv.* **2024**, *14*, 27873–27882.

[165] Yang, W.; Leng, T. C.; Miao, W. C.; Cao, X.; Chen, H. R.; Xu, F. F.; Fang, Y. M. Photo-switchable peroxidase/catalase-like activity of carbon quantum dots. *Angew. Chem., Int. Ed.* **2024**, *63*, e202403581.

[166] Zhang, Y. J.; Gao, W. H.; Ma, Y. N.; Cheng, L. L.; Zhang, L.; Liu, Q. G.; Chen, J. Y.; Zhao, Y. R.; Tu, K. S.; Zhang, M. Z. et al. Integrating Pt nanoparticles with carbon nanodots to achieve robust cascade superoxide dismutase-catalase nanozyme for antioxidant therapy. *Nano Today* **2023**, *49*, 101768.